NeuroImage 244 (2021) 118551

Contents lists available at ScienceDirect

NeuroImage

journal homepage: www.elsevier.com/locate/neuroimage

Capturing the non-stationarity of whole-brain dynamics underlying human brain states

J.A. Galadí[a,b,*], S. Silva Pereira[b], Y. Sanz Perl[c,d], M.L. Kringelbach[e,f,g], I. Gayte[a], H. Laufs[h], E. Tagliazucchi[c], J.A. Langa[a], G. Deco[b,i]

[a] Departamento de Ecuaciones Diferenciales y Análisis Numérico, Universidad de Sevilla, Spain
[b] Center for Brain and Cognition, Universitat Pompeu Fabra, Barcelona, Spain
[c] Buenos Aires Physics Institute and Physics Department, University of Buenos Aires, Argentina
[d] Laboratory of Experimental Psychology and Neuroscience, Institute of Cognitive and Translational Neuroscience, INECO Foundation, Favaloro University, Argentina
[e] Department of Psychiatry, University of Oxford, UK
[f] Centre for Music in the Brain, Department of Clinical Medicine, Aarhus University, Denmark
[g] Life and Health Sciences Research Institute (ICVS), School of Medicine, University of Minho, Portugal
[h] Department of Neurology, Christian-Albrechts-University Kiel, Germany
[i] Institució Catalana de la Recerca i Estudis Avançats (ICREA), Universitat Pompeu Fabra, Spain

ARTICLE INFO

Keywords:
Brain dynamics
Attractors
Energy levels
Sleep
Consciousness
Model transform

ABSTRACT

Brain dynamics depicts an extremely complex energy landscape that changes over time, and its characterisation is a central unsolved problem in neuroscience. We approximate the non-stationary landscape sustained by the human brain through a novel mathematical formalism that allows us characterise the attractor structure, i.e. the stationary points and their connections. Due to its time-varying nature, the structure of the global attractor and the corresponding number of energy levels changes over time. We apply this formalism to distinguish quantitatively between the different human brain states of wakefulness and different stages of sleep, as a step towards future clinical applications.

1. Introduction

High-dimensional complex systems usually exhibit a large number of attractors or stable steady states, and are thus far from thermodynamic equilibrium. The energy or *attractor landscape* (AL) characterizes all these states, limits the possible future behavior of the system, defines states with greater or smaller probability, and establishes the propensity of a system for more or less probable changes.

In Engineering and Mathematics, the AL can be represented within the Dynamical System Theory (DST) by means of a Lyapunov function, while in Physics the so-called *energy landscape* is usually expressed by means of a Potential function. Progress has recently been made in connecting both points of view (Yuan et al., 2014; Zhou et al., 2012).

However, to date this has not been applied to brain dynamics. Here, we develop a novel mathematical framework that allows us to capture for the first time the non-stationarity character of the attractor landscape of brain dynamics in different brain states.

A dynamical system is usually described by ordinary or partial differential equations -continuous time- or difference equations -discrete time-. Generally, the phase space of the system comprises the values of the dynamical variables. In DST, the *global attractor* is identified with a compact invariant subset of the phase space (Hale, 1988; Robinson et al., 2001). The global attractor determines the global asymptotic behavior of a *dynamical system*, i.e. it describes the past and the future of the system. The structure of the global attractor can be given in terms of isolated invariant subsets (typically, stationary points or periodic orbits) and the trajectories in phase space connecting them (Bortolan et al., 2020; Carvalho et al., 2012). According to DST, if the dynamical system supports a Lyapunov function, all isolated invariant subsets of the global attractor can be ordered by their level of attraction or stability. Then, a sequence of *energy levels* can then be defined (Aragao-Costa et al., 2012), and, for instance, dynamical systems with billions of stationary points in which detailed descriptions of the global attractor and the AL would not be available, can be characterized by just a few tens of energy levels. Indeed, the *number of energy levels* (NoEL) allows us to characterize the attractor landscape without having to calculate the explicit expression of a Lyapunov function or to estimate the Potential function (see Materials and Methods for details).

Traditional DST analysis focuses on the existence and local properties of a given steady state, but it does not explain the global dynamics

* Corresponding author at: Departamento de Ecuaciones Diferenciales y Análisis Numérico, Universidad de Sevilla, Spain.
E-mail address: jgaladi@us.es (J.A. Galadí).

https://doi.org/10.1016/j.neuroimage.2021.118551.
Received 24 March 2021; Received in revised form 22 August 2021; Accepted 1 September 2021
Available online 8 September 2021.

on complex systems in which transitions between attractors constitute the characteristic behavior. Brain dynamics do not converge or stabilize around a fixed set of invariants and might be described as a continuous flow of quick and irregular oscillations (Deco and Jirsa, 2012; Golos et al., 2016). Here, we propose to characterize the transitions between attractors by means of a *non-stationary attractor landscape*, that is, how the set of steady states and their connections evolve with time. Thus, a mathematical method to approximate the non-stationary attractor landscape is developed. To do this, we must rethink one of the central questions in computational neuroscience: the relationship between the human brain as a complex empirical system and the theoretical models expressed by means of equations. Usually, the parameters of the models are fitted in order to simulate general characteristics of the brain such as its functional connectivity or its metastability. However, whatever the values of the fitted parameters are, the attractor landscape offered by these models is static and the empirical transitions between attractors are still not well characterized.

Here we propose a new relationship between the model and the empirical data by means of the *model transform* (MT), which constitutes a useful tool to approximate the non-stationary landscape of complex systems. The MT is a newly developed concept (Galadí, 2020) which allows for the application of simple theoretical models to complex empirical systems in each short interval of time, and can be seen as a generalization of trivial concepts (such as the instantaneous velocity, the curvature or the torsion) when trivial models (the uniform motion in a straight line, the circumference or the helix) are applied in a small neighbourhood of the trajectory (see Materials and Methods for more details).

In summary, we search for the simplest model that will help us find an answer to the questions “towards which state is the brain attracted to at a given time point?” and “how do the corresponding attractor landscape surroundings look like?”, and we do so with help of DST. In the section Materials and Methods, we show that the model obtained is well known and called the Lotka-Volterra (LV) model.

Although it is not our intention to model neural activity, the LV equations have been previously used in neuroscience for this purpose: a LV equation for mean firing rate was derived from the conventional membrane dynamics of a neural network with lateral inhibition and self-inhibition in Fukai and Tanaka (1997); LV equations have been used to generate reproducible transient sequences in neural circuits (Afraimovich et al., 2004). It has been also shown that LV equations are capable of representing switching dynamics between different states of neural networks (Cardanobile and Rotter, 2011). The joint activity dynamics of excitatory and inhibitory populations has been analyzed employing a pair of mutually interacting nonlinear differential equations. In absence of a voltage leak for individual neurons and for negligible synaptic transmission delay, these equations take the form of LV equations (Lagzi et al., 2019; Lagzi and Rotter, 2015).

The Lotka-Volterra Transform (LVT) is the particular case of the MT when the harnessed model is the LV model. Thus, assuming time-varying growth rate parameters in the LV equations we obtain a time-varying AL (see Materials and Methods). The LVT can also be seen as a mathematical operator defined to exactly reproduce the empirical BOLD fMRI signals by finding the growth rate function that tracks their evolution over time. However, it is worth noticing that the equations are used to approximate the temporal evolution of the global attractor and the non-stationary attractor landscape, but *not* to model the temporal evolution of the system itself.

In order to explain the difference between modeling and the model transform, it should be underlined that each specific MT uses a specific model, but it is not modeling the system. Therefore, we do not attempt to make predictions of the dynamics in the short or long term. MT renounces the predictive power in exchange for defining new variables. Here, the final objective of MT is to define new measures, in this case measures of consciousness. MT is a generalization of the fact that there are simple models that extract certain information from a trajectory. One trivial example is the circumference, the simplest model which allows to calculate the curvature (the inverse of the radius of curvature) of any smooth curve at any point. But this does not mean that the whole smooth curve is shaped by a circumference. In this work, we do not state that the BOLD signals follow a LV system of differential equations. We just use a transformation to get well characterized non-stationary attractors. Non-stationary attractors should distinguish between awake and deep sleep states as a first partial validation to create a new measure of consciousness.

This innovative view relies on the fact that we are computing an asymptotic attractor at every time instant, i.e., the global attractor the system would achieve in the limit assuming a particular value of the growth rate parameter of the LV system. This is a more dynamical view of the problem not previously used in the literature, which let us adapt to the rich behaviour of brain dynamics.

Precisely by characterizing the AL by means of the number of energy levels, we are able to identify the different brain states. Over the last couple of years, there has been an increasing interest in trying to identify the necessary and sufficient properties of different brain states (Deco et al., 2019). Yet, thus far, there has been precious little progress in developing the necessary mathematical tools. Here, we propose the innovative non-stationary landscape approach to be assessed distinguishing between different human brain states as measured with neuroimaging. Developing such a framework would be a major step forward, potentially leading not only to a deeper understanding of the AL in different brain states but also to create sensitive and specific biomarkers characterising the brain states of individuals in wakefulness, deep sleep, anesthesia, or different levels of coma (Deco and Kringelbach, 2014). Obviously, this formalism is not needed to discriminate wakefulness and deep sleep, but the AL is of interest in itself. Our main aim is not to provide a better method to discriminate or to describe states of awake and sleep than those already existing in the scientific literature, but to validate, for the first time, a theoretical proposal based on the AL for the study of states of consciousness. Our method is justified as a first attempt to approximate the state the brain is drawn to at each time point and to calculate the corresponding non-stationary AL. In this sense, we are also interested here in characterising human sleep as a previous step towards future clinical applications to coma patients.

Human sleep is traditionally subdivided into different stages that alternate in the course of the night (Nir et al., 2013), mainly non-rapid-eye-movement (NREM) and rapid-eye-movement (REM) sleep. NREM is further subdivided into light sleep (N1), NREM sleep stage (N2) and NREM deep sleep stage (N3). From N1 to N3, traveling brain waves become slower and more synchronized.

In this study, we aim to 1) associate brain states with the average and variability of the number of energy levels (NoEL) of the AL across time and to 2) demonstrate that this mathematical formalism can be applied to distinguish quantitatively and rigorously between the different brain states of wakefulness and deep sleep using state-of-the-art neuroimaging data collected from healthy human participants.

1.1. Motivations

The first motivation for this work is based on the thesis that the fundamental information of a dynamical system is expressed in the structure of its global attractor. One consequence of this thesis is that, in the case of the human brain as a dynamical system, the structure of the attractor could be related to the corresponding states of consciousness. Hence the importance of finding a method to approximate the attractor of brain dynamics and its testing in different states of consciousness.

Note that we go from BOLD fMRI signals to a flow of ALs and its abstract structures. We consider of high interest to show that this flow of structures is informative about states of consciousness. Thus, another objective of our method is to define new measures of consciousness. Although we are not trying to improve other current methodologies for classification to distinguish among states of consciousness, we believe

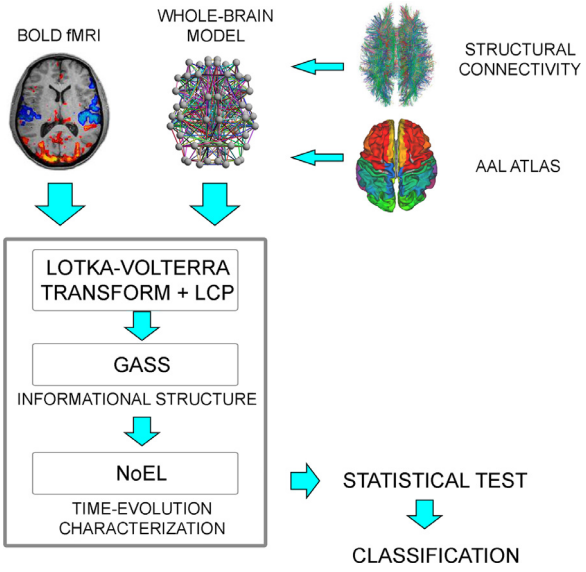

Fig. 1. Flowchart illustrating the methods. For this study, we used an automated anatomical labelling (AAL) atlas. The Lotka-Volterra transform, constrained by the whole-brain model, is a mathematical operator that calculates the growth rate as a function that exactly reproduces the filtered empirical BOLD fMRI signals. Then, solving the linear complementarity problem (LCP) we calculate the globally asymptotically stable stationary solution (GASS) and the number of energy levels (NoEL) of the attractor landscape at each time instant. In order to assess how different the distributions of the NoEL for awake and for deep asleep are, we calculate a statistical hypothesis test (Wilcoxon test) and the J_{ind} (see Supplementary Materials for a more detailed flowchart) before classification.

this new perspective opens the door to further detailed studies, so that it could serve as the seminal work for a full research plan. The novelty of this approach is essentially a first transformation of BOLD data into a non-stationary description of the brain attractor landscape by a dynamical system approach. Even beyond neuroscience and on the side of mathematical DST, this way to interpret attractors as an instantaneous object is also new.

Another of the motivations for this work is the search for a method to calculate the empirical "ghost" attractors of the resting (and sleep) state suggested in Deco and Jirsa (2012), Vohryzek et al. (2020). The resting state dynamics needs to be explained, and these attractors would correspond to distinct foci of high activity in particular brain areas. According to Deco and Jirsa (2012), at the edge of the transition from resting state to task context the local attractors would not exist as stable fixed points yet, since they are either saddle points, or regimes with close to zero flow in the phase space. However, as a possible neurobiological explanation of the resting state dynamics, these states could be easily stabilized when needed in a given task context or for a given function. We believe that our new formalism could be used to detect empirical ghost attractors since, in a non-stationary AL, stable attractors are never reached. Thus, they are candidates to play the role proposed in Deco and Jirsa (2012) in the sense that brain dynamics seem to be attracted to them, which can further be interpreted as latently attracting the system and potentially stabilizable in transitions from resting state to specific tasks.

2. Materials and methods

2.1. Overview of the method

We aim to characterize the different brain states of wakefulness and deep sleep by approximating the non-stationary *attractor landscape* (AL) as shown in Fig. 1 with the flowchart of steps. Briefly, first we enter in the *Lotka-Volterra* (LV) equations

$$\dot{u}_i = u_i\left(\alpha_i - u_i + \sum_{j\neq i}^{n}\gamma_{ij}u_j\right), i = 1,\dots,n,$$

the structural connectivity matrix (SCM) between $n = 90$ standardized brain areas through an automated anatomical labelling (AAL) atlas (Tzourio-Mazoyer et al., 2002) as the γ_{ij} parameters, which are obtained by applying tractography algorithms to diffusion magnetic resonance imaging (dMRI).

Second, we applied the *Lotka-Volterra Transform* (LVT)

$$\alpha_i(t) = \frac{\dot{u}_i(t)}{u_i(t)} + u_i(t) - g\sum_{j=1}^{n}\gamma_{ij}u_j(t), i = 1,\dots,n.$$

to calculate the growth rate $\alpha(t)$ that reproduces exactly the filtered empirical BOLD fMRI signals $u_i(t)$. Both $u(t)$ and $\dot{u}(t)$ are empirical values in the form of discrete time series. The global coupling strength parameter g will be fitted to balance information from the proper region i, $\frac{\dot{u}_i(t)}{u_i(t)} + u_i(t)$, and information from the rest of the brain $\sum_{j=1}^{n}\gamma_{ij}u_j(t)$.

Third, we characterize the corresponding attractor landscape computing the globally asymptotically stable stationary solution (GASS) and the *number of energy levels* (NoEL) at each time instant t^* solving

$$\dot{u}_i = u_i\left(\alpha_i(t^*) - u_i + \sum_{j\neq i}^{n}\gamma_{ij}u_j\right), i = 1,\dots,n.$$

Finally, in order to assess differences in the ALs between wakefulness and deep sleep, we use the non-parametric Wilcoxon signed-rank test and the J index. We consider two quantitative descriptors of the ALs, the time average of NoEL ($\overline{q}$) and the standard deviation of NoEL (σ_q), both calculated for each participant in the two brain states. We obtained the p-value of a paired and two-sided test for the null hypothesis that the distribution of average NoEL (or their standard deviation) presented the same median during awake vs. deep asleep subjects. In addition, we defined the following measure J_{ind} :

$$J_{\text{ind}} = \frac{\sum_{i=1}^{ns}(\overline{q}_{as,i} - \overline{q}_{aw,i})}{\sum_{i=1}^{ns}|\,\overline{q}_{as,i} - \overline{q}_{aw,i}\,|} \quad (1)$$

where ns is the total number of subjects, $\overline{q}_{as,i}$ is the value of $\overline{q}$ for subject i while asleep and $\overline{q}_{aw,i}$ is the value of $\overline{q}$ for subject i while awake. Then, $J_{\text{ind}} = 1$ ($J_{\text{ind}} = -1$) if the mean number of energy levels is larger (smaller) for deep sleep than wakefulness for all subjects and $J_{\text{ind}} \simeq 0$ if the null hypothesis holds. Please note that J_{ind} can also be defined for σ_q or for any other parameter (see Supplementary Materials for more details).

2.2. BOLD signal acquisition

In order to compare different naturally occurring brain states we use data from 18 healthy participants: specifically, BOLD fMRI signals in resting state and asleep phases (N1, N2 and N3). Empirical data comes from a set of fifty-five subjects (thirty-six females, mean ± standard deviation age of 23.4 ±3.3 years) who fell asleep during a simultaneous EEG-fMRI recording previously described in Tagliazucchi and Laufs (2014), where 18 participants who reached stage N3 sleep (deep sleep) were selected. The mean duration (±standard deviation) of contiguous N3 sleep epochs for these participants was 11.67 ± 8.66 min. fMRI data was recorded at 3T (Siemens Trio, Erlangen, Germany) simultaneously with EEG data using an MR-compatible EEG cap (modified BrainCapMR, Easycap, Herrsching, Germany), MRI-compatible amplifiers (BrainAmp MR, BrainProducts, Garching, Germany), and sleep stages were scored manually by an expert according to the AASM criteria (AASM, 2007).

2.3. BOLD signal preprocessing

fMRI data was realigned, normalized and spatially smoothed using SPM8 (www.fil.ion.ucl.ac.uk), (see Tagliazucchi and Laufs, 2014 for

full acquisition, pre-processing and sleep scoring details). Cardiac (with frequencies around $1 \sim 2$ Hz), respiratory (around 0.3 Hz), motion-induced and their temporal aliasing noises were regressed out from the fMRI BOLD signals, and data were band-pass filtered in different ranges.

Empirical BOLD signals are generally band-pass filtered to remove the contribution of noise. In this study we take a particular look at this process to better illustrate how the attractor landscape found in resting state and in the deep sleep differentiate from each other. Different filters have been proposed in the literature to obtain the most reliable results. We consider all the possible filters below the Nyquist frequency to show how the non-stationary landscapes differ in awake and asleep conditions.

2.4. Structural connectivity matrix

For the whole-brain network model, the interactions between the 90 brain areas were scaled in proportion to their white matter structural connectivity. For this study, we used the structural connectivity between the 90 automated anatomical labelling (AAL) regions obtained in a previous study (Deco et al., 2017) averaged across 16 healthy young adults (5 females, mean ± SD age: 24.75 ± 2.54). Briefly, for each subject, a 90×90 structural connectivity matrix $\Gamma = [\gamma_{ij}]$ was obtained by applying tractography algorithms to Diffusion magnetic resonance imaging (dMRI) where the connectivity γ_{ij} between regions i and j was calculated as the proportion of sampled fibers in all voxels in region i that reach any voxel in region j. Since dMRI does not capture fiber directionality, γ_{ij} was defined as the average between γ_{ij} and γ_{ji}. Averaging across all 16 participants resulted in a structural connectivity matrix Γ representative of healthy young adults. We ordered the different brain areas in the neuroanatomical connectivity matrix in such a way that homotopic regions in the two cerebral hemispheres were arranged symmetrically with respect to the center of the matrix (see Supplementary Materials for details).

2.5. Global attractor and energy levels

The global attractor (see Supplementary Materials for a formal definition) is usually comprised of isolated invariant subsets and trajectories connecting them (Carvalho et al., 2012). The highest energy level is defined as formed by isolated invariant subsets that receive no solution, i.e. unstable or source sets. Then, each successive lower level is defined including those isolated invariant subsets that receive solutions only from the previously defined higher levels (Aragao-Costa et al., 2012).

These concepts can be illustrated using the Lotka-Volterra (LV) system as follows:

$$\dot{u}_i = u_i\left(\alpha_i - u_i + \sum_{j\neq i}^{n} \gamma_{ij}u_j\right), i = 1, \ldots, n, \tag{2}$$

where α_i are the growth rates and γ_{ij} the structural connectivity, both considered constant in time. This is an example of a dynamical system on a network where the conditions for existence and uniqueness of solutions are well-known (Murray, 2013). An shown in the example of Fig. 2A–C with $n = 2$, with suitable γ_{ij} and α_i there are four stationary points (i.e. four isolated invariant subsets): one located at the origin ($u_1 = 0, u_2 = 0$), one at the x-axis ($u_1 \neq 0, u_2 = 0$), one at the y-axis ($u_1 = 0, u_2 \neq 0$), and one at the positive quadrant ($u_1 \neq 0, u_2 \neq 0$). The stationary points of the LV system for $n = 2$ can be described as two binary variables, null values indicating that the corresponding dynamical variable is zero (i.e. is located in one of the axes), and non-null values indicating that it is located outside that axis. In other words, the global attractor of the system (and thus its asymptotic behavior) could be encoded as a set of Boolean variables and connecting global solutions among them.

Figure 2 C shows that the stationary points are partially ordered, i.e. they admit an order relationship in which not necessarily all the pairs of elements can be compared. In this ordering, the unstable and stable points are maximal and minimal respectively, with the two other stationary points (saddle points) not being ordered with respect to each other. Thus, there are three energy levels: the trivial solution (unstable point), the saddle points, and the stable solution. The number of energy levels (NoEL) q will be the most important parameter in our data analysis (see Supplementary Materials for more details and formal definitions).

Figure 2 D–F show a LV system for $n = 4$ where $\alpha_i \;\; i = 1, \ldots, 4$, are now periodic functions of time. Changes in the α_i produce changes in the AL so that the NoEL q also changes over time. For LV systems, each energy level is formed by stationary points with the same number of non-zero components, and the only stable point is a single stationary point in the lowest level with incoming solutions only, called globally asymptotically stable solution (GASS). The GASS is the point the system is attracted to, since any initial point of $\mathbb{R}^n_+$ will converge to the GASS (Takeuchi and Adachi, 1980).

It can be shown that there exists an equivalence between obtaining the GASS of LV systems and solving a linear complementarity problem (LCP, see Takeuchi, 1996 and Supplementary Materials). Furthermore, the NoEL q equals the number of non-zero entries in the GASS plus one (see Fig. 2F). The LCP associated with the LV can be solved using the Complementary Pivot Algorithm (Cottle et al., 1992). Although the LV model is relatively simple, with $n = 90$ nodes it could include a complex AL with up to 2^{90} (1.238×10^{27}) stationary points.

The *Informational Structure* (IS) of the global attractor is defined as a directed graph composed of nodes associated with the isolated invariant subsets and links establishing their connections (see Fig. 2C and F, and Supplementary Materials for a formal definition).

2.6. Model transform

A formal definition of the *Model Transform* (MT) is provided in the Supplementary Materials. In short, the idea is the same as when a uniform motion in a straight line is fitted to any three-dimensional motion in an arbitrarily small segment of the trajectory. If we want to quantify how a motion $\vec{x}(t)$ "moves away from rest", we must look for the simplest possible motion that allows us to measure that distance. Simple motion in this case is the uniform motion in a straight line and, adjusting it to each small neighborhood of $\vec{x}(t)$, the variation per unit of time of $\vec{x}(t)$ is a measure of "remoteness from rest". Therefore, we say that the uniform motion in a straight line is the minimum model that transforms a motion $\vec{x}(t)$ into $\vec{v}(t)$, or conversely that $\vec{v}(t)$ is the MT of $\vec{x}(t)$ when the minimum model is uniform motion in a straight line. Note that first, we have an intuitive idea of what we want to measure and then, after choosing a minimal model, the intuitive idea is specified and formalized. Thus, the equations $x_i'(t) = v_i, i = 1, 2, 3$ can be seen as a "model" of uniform motion in a straight line when v_i has a fixed value for $i = 1, 2, 3$ or, alternatively, they can be seen as a definition of the instantaneous velocity $\vec{v}(t)$ at each time point t for any trajectory $\vec{x}(t)$. In the latter case, the value of $\vec{v}$ changes over time and the MT transforms $\vec{x}(t)$ into $\vec{v}(t)$. The $\vec{v}(t)$ can also be seen as defined to exactly reproduce $\vec{x}(t)$ integrating $x_i'(t) = v_i(t), \;\; i = 1, 2, 3$ when the initial point $\vec{x_0} = \vec{x}(t_0)$ is known. The uniform motion in a straight line is the simplest model that allows us to know "how far an object moves from rest at each time instant" using the model parameters $v_i, \;\; i = 1, 2, 3$.

In summary, we look for the simplest model that allows us to answer the questions "towards which state is the brain attracted to at one time point?" and "how is the attractor landscape characterized at one time point?". These questions are answered with help of the DST. Mathematically speaking, the Lotka-Volterra model is the simplest nontrivial cooperative model which includes the trivial solution $(0, 0, \ldots, 0)$ and possesses a GASS. Models of global brain dynamics are usually cooperative in the sense that different brain areas act cooperatively (excitation), while there is inhibition only at local level (within each region). The inclusion of the trivial solution and the GASS are crucial in our study of the attractor structure, since they both mark the beginning and the end

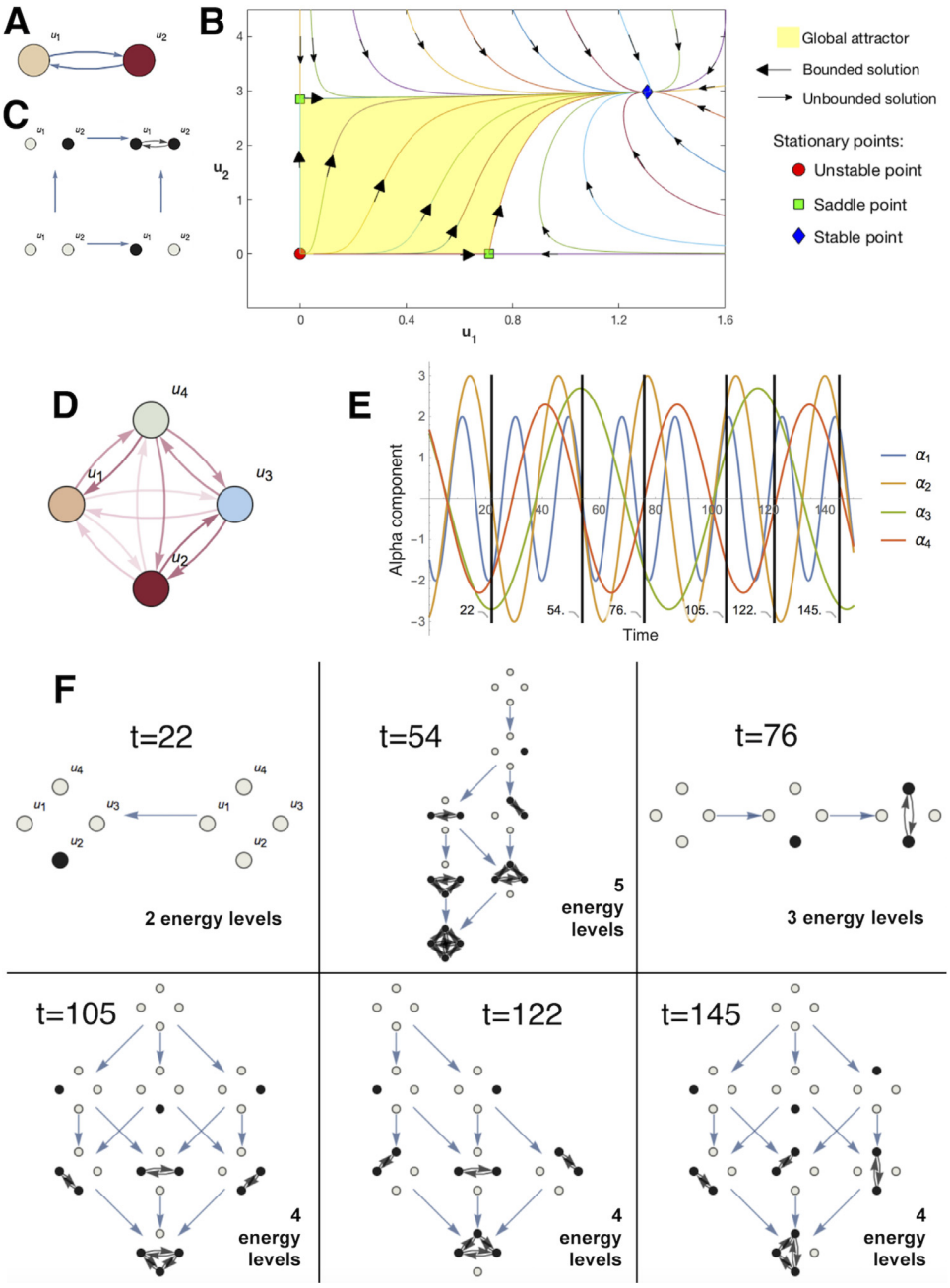

Fig. 2. (**A**), Two-node structural network of a Lotka-Volterra (LV) system (2), with $\alpha_1 = 0.71$, $\alpha_2 = 2.85$, $\gamma_{12} = 0.2$ and $\gamma_{21} = 0.1$. (**B**), Solutions of the LV system in **A**. The global attractor is the set of all bounded solutions (yellow area).(**C**), The structure of the global attractor is a new network made by four nodes associated with the four stationary points and directed links associated with connecting solutions. The relation induced by the links is transitive such that only the minimal links are represented. Each node of this graph is represented as a subgraph of the original LV system where non-null components are shown in black and null in grey. In this example there are three energy levels: the trivial solution, the saddle points, and the stable solution. (**D**), Structural network of a 4-dimensional ($n = 4$) LV system (see Supplementary Materials for γ values). (**E**), In this example α_i are periodic functions of time. (**F**), Structures of the global attractor corresponding to time steps shown in **E**. The number of energy levels (NoEL) changes over time, and equals the number of non-zero entries in the lowest level plus one. (For interpretation of the references to colour in this figure legend, the reader is referred to the web version of this article.)

of said structure; that is, both the first and the last energy levels, along with the "distance" between them give us the NoEL.

Furthermore, we show (see Supplementary Materials) that the Lotka-Volterra model:

i) includes a rich attractor landscape with a large number of stationary points, which are a unique combination of active and inactive nodes of the dynamical system,
ii) includes empirical information regarding the structural connectivity of the dynamical system,
iii) has a well-known condition for existence and uniqueness of the state the system is attracted to, i.e. the GASS,
iv) supports a Lyapunov function so that its isolated invariants could be ordered according to the energy levels,
v) supports an algorithm of low computational complexity (the Complementary Pivot Algorithm for solving the LCP), so that
vi) the global attractor has a well-known structure.

The Lotka-Volterra Transform (LVT) is the particular case of MT when the model is given by the LV equations:

$$\dot{u}_i = u_i\left(\alpha_i - u_i + g\sum_{j=1}^{n}\gamma_{ij}u_j\right), i = 1, \dots, n, \tag{3}$$

where g is a global coupling strength parameter. From these equations we can obtain time-dependent parameters $\alpha_i(t)$ as follows:

$$\alpha_i(t) = \frac{\dot{u}_i(t)}{u_i(t)} + u_i(t) - g\sum_{j=1}^{n}\gamma_{ij}u_j(t), i = 1, \dots, n. \tag{4}$$

This expression defines the LVT.

Finally, we can associate each parameter and variable of the LVT with its neurobiological counterpart: both $u(t)$ and $\dot{u}(t)$ will be empirical values from BOLD fMRI signals in discrete form; structural connectivity information in γ_{ij} will be obtained by applying tractography algorithms to diffusion magnetic resonance imaging (dMRI) where the connectivity

between regions i and j is calculated as the proportion of sampled fibers in all voxels in region i that reach any voxel in region j; the global coupling strength parameter g will be fitted to balance information from the proper region i, $\frac{\dot{u}_i(t)}{u_i(t)} + u_i(t)$, and information from the rest of the brain $\sum_{j=1}^{n} \gamma_{ij} u_j(t)$. LVT transforms $u(t)$ into $\alpha(t)$, i.e., LVT transforms empirical data into auxiliary functions $\alpha_i(t)$.

2.7. Alternative model transforms

Given a dataset like ours, with resting state and N3 deep sleep data, can any model transform differentiate between these states? In the search for biomarkers of consciousness, what does the LVT contribute with, compared to any other MT?

We use four generative models possessing various levels of complexity: i) the Kuramoto model for coupled oscillators, ii) the simultaneous autoregressive (SAR) model, a purely spatial model with no dynamics that expresses BOLD fluctuations within one region as a linear combination of the fluctuations in other regions, iii) a rate fluctuations model, which is a simplified version of the Wilson–Cowan system considering exclusively the excitatory population, and iv) the Lotka-Volterra (LV) model.

The Kuramoto model Kuramoto (1975), Yeung and Strogatz (1999) consists of a set of coupled oscillators:

$$\frac{d\phi_i(t)}{dt} = \omega_i + g \sum_{j \neq i} \gamma_{ij} sin(\phi_j(t) - \phi_i(t))$$

where ϕ_i and ω_i stand for the phase and intrinsic angular frequency of region i. g and γ_{ij} are defined as in the LV model.

The simultaneous autoregressive (SAR) model is composed of a linear combination of the fluctuations within other regions (Tononi et al., 1994):

$$u_i = g \sum_{j \neq i} \gamma_{ij} u_j + \nu_i$$

where ν_i stands for uncorrelated white Gaussian noise, and u_i, g and γ_{ij} are defined as in the LV model.

The Rate fluctuations model (Galán, 2008) is a simplification of the Wilson–Cowan model where inhibitory neurons and saturation have been removed:

$$\tau \frac{du_i(t)}{\mathrm{d}t} = -u_i(t) + g \sum_{j \neq i} \gamma_{ij} u_j(t) + \nu_i.$$

Here, τ is the time scale of the excitatory population, and ν_i stands for uncorrelated white Gaussian noise. u_i, g and γ_{ij} are defined as in the LV model.

Specifically, to test which model stands out compared to the others when it comes to finding differences between brain states, we contrast the four different model transforms (MT) to validate the choice of LV. Always starting from the same dataset, we look for the model with greatest capacity to distinguish between states of consciousness. In order to test this capacity, we add the sign test and the paired t-test (for more details see Supplementary Materials) to the non-parametric Wilcoxon signed-rank test and the J index. The models that we compare with LV have shown high predictive power of the functional connectivity starting from the structural connectivity (Messe et al., 2015).

To calculate the Kuramoto Transform (KT), we previously perform a Hilbert transform (Marple, 1999) of the BOLD signal to obtain the amplitude and phase of the signal. ϕ_i is now said empirical phase in each region i. ω_i is the parameter of the model that becomes a function of time and that will be the actual result of the KT:

$$\omega_i(t) = \frac{d\phi_i(t)}{dt} - g \sum_{j \neq i} \gamma_{ij} sin(\phi_j(t) - \phi_i(t)).$$

For the SAR Transform (SART), ν_i is the model parameter that is converted to a function of time. Therefore, instead of being modeled as a Gaussian noise, it is calculated exactly from the experimental data:

$$\nu_i(t) = u_i - g \sum_{j \neq i} \gamma_{ij} u_j$$

In the Rate fluctuations Transform (RFT), ν_i is again the chosen parameter:

$$\nu_i(t) = \tau \frac{du_i(t)}{\mathrm{d}t} + u_i(t) - g \sum_{j \neq i} \gamma_{ij} u_j(t).$$

For details about these model transform processes, see Supplementary Materials.

3. Results

3.1. Impact of free parameters

We transform time series of BOLD signal data of 18 healthy participants into time series of attractor landscapes (ALs), and investigate the distribution of the number of energy levels (NoELs) of the AL during wakefulness and deep sleep. Although the α_i become time-varying and are fitted in each small time interval, other parameters remain free and we study their impact on the classification of brain states.

Impact of coupling strength: The strength of the connections between pairs of nodes is controlled by the coupling strength parameter g. Changes in coupling strength g lead to changes in α, and therefore have an impact on the distribution of NoEL. Figure 3A shows the impact of g on the ability of AL to differentiate between the two brain states, i.e., showing how the gap between awake and deep asleep changes as a function of g. A vertical dashed line shows the maximum value ($g < 0.36743$) ensuring global stability. We compute the Pearson linear correlation coefficient between the two curves (−0.9781) to corroborate that the J_{ind} basically measures the same as the Wilcoxon test (although J_{ind} is more intuitive and easier to calculate). The optimal value ($g = 0.29$) is the same in both tests, and therefore we choose it for our computations. Note however, that the gap between awake and asleep is not restricted to this value. Indeed, the range of g in which the differences between the distributions of energy are manifest (p-values below 1% or 10^{-2}) is very broad. In Fig. 3A we can see that there is a wide range of values for which the p-value is small (from around $g = 0.05$ to the red dashed line in $g = 0.36743$, where global stability of the system is guaranteed). In that same interval J_{ind} remain above 72% ($J_{\mathrm{ind}} = 0.72$). In other words, our results are robust, as they do not depend on a specific value of g. In addition we verified (Fig. 3A) that the suggested method does not produce good results when the information from the coupling term in the LVT is not considered, i.e. g tends to zero. At the other extreme, when g tends to its maximum value the LVT does not distinguish so well between brain states. We can state that our method's ability to distinguish brain states only decreases when global connectivity is too small or too large.

Impact of time series filtering: Fig. 3B shows the results of the Wilcoxon test and J_{ind} index for the mean $\overline{q}$ and the standard deviation σ_q of the NoEL assuming different filter ranges. At high frequencies, noise was not filtered and the ALs of the two brain states were very similar, the p-value was high and the J_{ind} small. For $\overline{q}$, the filter range with minimum p-value was 0.077 – 0.096 Hz ($p = 0.00023$). For σ_q, the filter range with minimum p-value was 0.077 – 0.106 Hz ($p = 0.00023$) and the second best was 0.077 – 0.096 Hz (p-value= 0.00028). For σ_q, the filter range with maximum J_{ind} was 0.077 – 0.106 Hz ($J_{\mathrm{ind}} = 0.9954$) and the second best was 0.077 – 0.096 Hz ($J_{\mathrm{ind}} = 0.9813$). Therefore, we chose the filtering range 0.077 – 0.096 Hz. When the signal was filtered in this range, the difference between the distributions of NoEL and therefore, between the ALs of awake and sleeping participants, is maximal. The values obtained for most filters (wide filters, narrow filters or even filter absence, i.e. 0.0 – 0.24 Hz where 0.24 Hz is the Nyquist frequency) were good enough ($J_{\mathrm{ind}} > 0.75$ and p-value< 0.01) to sustain that our results can not be attributed to a specific filter. Rather, we demonstrated that our

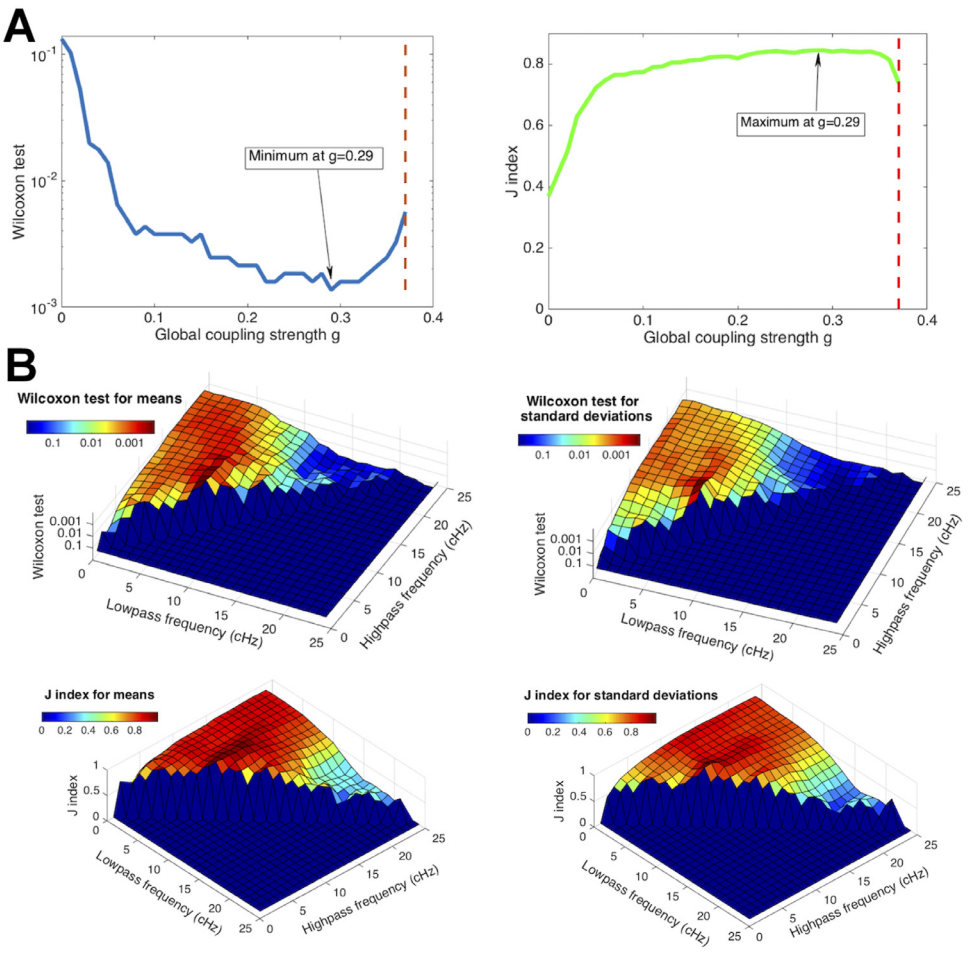

Fig. 3. (**A**), Impact of coupling strength g on the p-value of the Wilcoxon test and the J_{ind} maximization, both for mean NoEL. The red dashed line ($g < 0.36743$) delimits the region in which global stability is guaranteed. In both cases the optimal value is $g = 0.29$. (**B**), Impact of the filter used on the p-value of the Wilcoxon test and the J_{ind} for the samples of both, $\bar{q}$ and σ_q. Both, the Wilcoxon test p-value and the J_{ind} are functions of the ends of the filtering range (see Supplementary Materials for a 2D version of the graphics).. (For interpretation of the references to colour in this figure legend, the reader is referred to the web version of this article.)

hypotheses, in general, were true even for the unfiltered signal. Only high-pass filters provided negative results ($J_{\text{ind}} < 0.4$ and $p > 0.2$). Thus, our conclusions are again robust in this regard.

3.2. Statistical analysis of non-stationary attractor landscapes

The Lotka-Volterra Transform (LVT) allows us to compute the time-varying vector α for every participant in both brain states. Using the linear complementarity problem (LCP) we computed the globally asymptotically stable solution (GASS).

Figure 4 A shows a 208-seconds long sample of the NoEL as a function of time for one subject in awake state and deep sleep state. We studied the NoEL distributions for the 18 participants in both conditions. Generally, the NoEL increased when the components of alpha grow (Fig. 4B, where alpha components were computed using the LVT).

In order to draw general conclusions beyond the inter-individual differences, we computed the average distribution of the 18 participants in the awake state and the average distribution of the 18 participants in the sleep state (Fig. 4C). The pattern typically observed was that the distribution for the awake state was more homogeneous along $q \in [1, 80]$ NoEL values. ALs with extreme NoEL values (that is, low: < 28, or very high: 90 or 91), were more frequent in awake individuals.

Figure 4 D shows the mean NoEL $\bar{q}$ in awake vs. deep asleep (N3) with filtered signals in the range 0.077 – 0.096 Hz. The error bars were computed according to $error = \sigma_q / \sqrt{T}$ where σ_q is the standard deviation of the NoEL and T was the length of the data series. For all participants except one, the mean NoEL $\bar{q}$ was higher when the participants were in deep sleep. In order to assess how different $\bar{q}$ is for participants in awake and deep sleep, we use the signed-rank test Wilcoxon and we obtain $p = 0.00023$, i.e., differences between the means of both brain states are significant. In addition, we compute $J_{\text{ind}} = 0.9948$. Recall that $J_{\text{ind}} = 1$ when $\bar{q}$ is larger for all participants in the deep sleep state.

Then, we establish patterns regarding the variability of the distributions. We compute the standard deviations of the distribution of NoEL in each participant for the two brain states. In Fig. 4E each point represents a participant. The error bars were calculated according to the standard error of the standard deviation

$$\frac{1}{2\sigma}\sqrt{\frac{1}{T}(\mu_4 - \frac{T-3}{T-1}\sigma^4)} \tag{5}$$

where σ is the standard deviation of the NoEL, T is the length of the data series, and $\mu_4 = E(q - \bar{q})^4$ Rao (2009). For 17 (out of 18) participants the standard deviation is larger for wakefulness than for the deep sleep state, $J_{\text{ind}} = -0.9813$ and $p = 0.00028$. Again, the differences between the standard deviations of both brain states are very significant. There is only one participant who shows a greater deviation when asleep. This may be more clearly understood recalling Fig. 4C, where ALs with extreme NoEL values are more frequent in awake individuals.

3.3. Comparison including N1 and N2

Results of the analysis of data from N1 and N2 states are included in Fig. 5A–C. where N1, N2 and N3 states are significantly ordered according to statistical tests (Fig. 5D) so that, as deeper levels of sleep are reached, the average NoEL increases while the standard deviation decreases. However, the differences between awake and N1 are not significant neither for the mean nor for the standard deviation (Fig. 5D-E). The same is true for the comparison between awake and N2 (Fig. 5D and F). Nevertheless, the NoEL distributions distinguish between these

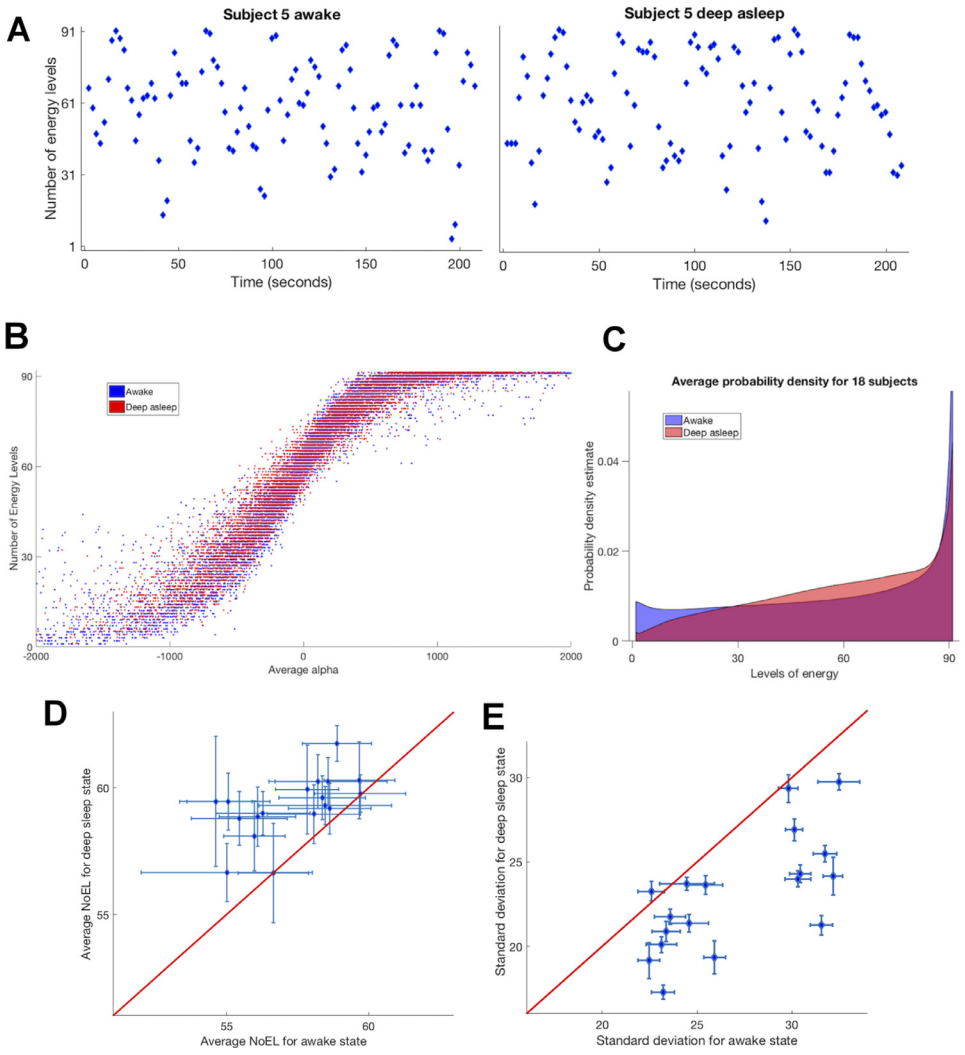

Fig. 4. (**A**), Sample of 208 seconds of the number of energy levels (NoEL) for participant number 5 in wakefulness and deep sleep states (filter $0.01 - 0.1$ Hz, $g = 0.29$). (**B**), Number of Energy Levels (NoEL) as a function of the average 90 alpha components (same g as before). Each dot represents a time point of a subject in a brain state. (**C**), Average distribution of the NoEL for 18 healthy participants in awake and in deep sleep states (see Supplementary Materials for individual histograms). (**D**), Average number of energy levels $\bar{q}$ of 18 participants awake vs. deep asleep (N3) ($J_{\text{ind}} = 0.9948$, $p = 0.00023$). $\bar{q}$ is the same for wakefulness and for deep sleep brain states along the red line. (**E**), Standard deviation of the NoEL for deep asleep state vs. wakefulness state. ($J_{\text{ind}} = -0.9813$, p-value= 0.00028). In graphics **B-E** the NoEL was obtained from filtered data between $0.077 - 0.096$ Hz (see Supplementary Materials for a similar figure using other filters).. (For interpretation of the references to colour in this figure legend, the reader is referred to the web version of this article.)

states: Fig. 5G shows the NoEL distribution averaged across the four states (awake, N1, N2 and N3) and the 18 subjects (inset), as well as the differences between the average distributions for each state with respect to the mean. We observe that the differences between states are more significant for certain NoELs. Thus, if we compare the frequency at which the AL reaches 15 levels in each of the 18 subjects for awake and N1 states, the differences are significant (Fig. 5H). The same is true when we compare the frequency at which the AL reaches 13 levels in the comparison between awake and N2 states (Fig. 5I). Further observations show that the average NoEL for five subjects shows a monotonic increase from awake to N3 sleep, whereas another four subjects shows the same monotonic increase but with lower average NoEL in N1 than in the awake state (see Supplementary Materials).

3.4. Comparison of model transforms

We contrast different model transforms (MT) and show that LV stands out compared to other models when it comes to finding differences between brain states (Fig. 6A–E). The MTs for four different models (LV model, SAR model, Rate fluctuations model and Kuramoto model) are compared and validate the choice of LV. We use the same dataset for all MTs and start filtering the BOLD signals in the range $0.077 - 0.096\,Hz$. g was optimized in each MT to find the greatest differences between brain states. The results show that LV has a greater capacity to distinguish between states of consciousness than the other models.

In our formalism, we transform the BOLD signals into alpha values using the LVT and then use these alphas to calculate the structure of the corresponding attractor, along with its energy levels. Figure 6F compares the ability of alphas with the ability of NoEL to distinguish states of consciousness. The result is that the structure of the attractor through its energy levels is able to distinguish between states much better, so the simple calculation of the alphas would not be enough to generate a measure of consciousness.

3.5. Classification

In addition, we have classified the subjects by training a KNN classifier with $k = 2$, obtaining high percentages of accuracy with minimal amounts of training data. Leave-one-out cross-validation and Receiver Operating Characteristics (ROC) analysis are included in this classification process. Figure 6G–H shows the classification results training the classifier with the mean and the standard deviation of the NoEL of 36 subjects (18 in N3 and 18 in awake resting state). The area under the curve (AUC= 0.89) is a performance measure of our classification problem at various threshold values: it indicates how much our formalism is capable of distinguishing between brain states. The higher the AUC, the better the formalism to predict N3 subjects as being in N3 and awake subjects being awake. By analogy, the higher the AUC, the better to distinguish between brain states.

Thus, subjects can be classified with an accuracy of 89% by training the classifier with only the standard deviation of the NoEL. If we add

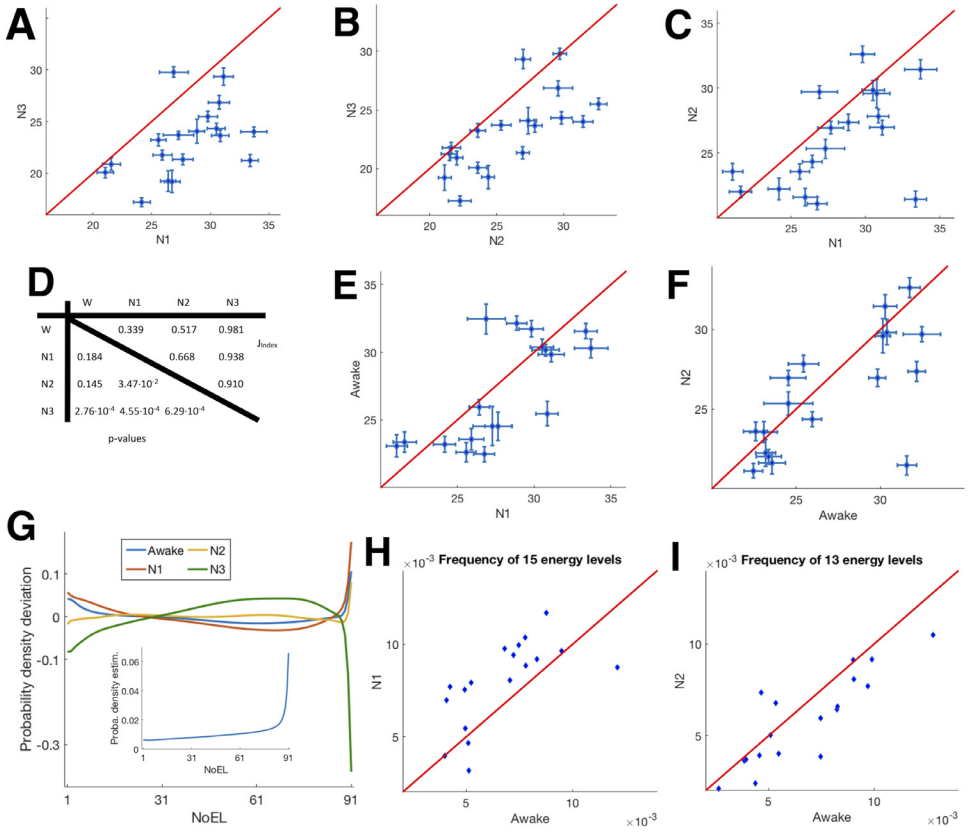

Fig. 5. (**A–F**), Comparisons of NoEL standard deviation among awake, N1, N2 and N3 (deep asleep) states (see Fig. 4 for awake-N3 comparison). Error bars were calculated according to (5) (**D**), J_{ind} and p-values of the Wilcoxon tests. The differences between N1, N2 and N3 were very significant (p-values< 5%), but differences between awake and N1 or N2 were not significant (see Supplementary Materials for comparisons of average NoEL). (**G**), Deviation of the NoEL distribution of each state respect to average NoEL distribution (inset) of the four states. (**H**), Frequency of attractor landscapes (ALs) of 15 energy levels of 18 participants awake vs. N1 (J_{ind} =0.6629, p = 0.0139). (**I**), Frequency of ALs of 13 energy levels of 18 participants awake vs. N2 (J_{ind} =0.6418, p = 0.0139). In all graphics (A-I) the NoEL was obtained from filtered data between 0.077 – 0.096 Hz.

the mean NoEL, the accuracy rises to 92% as shown in Fig. 6G. It is noteworthy that the classifier can be trained with particular values of the NoEL distribution (instead of global characteristics of the distribution like mean and standard deviation) such as the frequency of a given NoEL level. For instance, with the frequency of level 59, an 89% accuracy is obtained. Moreover, if we add the frequency of level 3, the accuracy rises further to 92%.

3.6. Attracting brain areas

Next, we investigated which areas were active (non-zero components) in the attractor (GASS). On average, the attractor of the deep sleep state was more populated (larger NoEL) than that of the wakefulness state. Hence, most of the brain areas tended to appear more frequently in the deep sleep attractor than in the wakefulness attractor. In other words, as $\bar{q}$ was greater in the participants in deep sleep, the general tendency was that each area of the brain was more frequently present in the deep sleep attractors than in the wakefulness attractors (with some exceptions). As shown in Fig. 7AB, we computed the frequency of appearance of an area in the GASS for each participant and for each brain state, averaged over all participants, and then we computed the difference between the frequencies in awake and in deep sleep states for each participant and area (Fig. 7C). As can be seen, most of the areas showed less presence in the wakefulness attractor than in the deep sleep attractor. But there were some exceptions (indicated by the warm colours), i.e., greater presence of the area in the wakefulness attractor (see Supplementary Materials for individual differences, where we found inter-individual variability but, in all cases, warm colors were exceptional).

Considering the averaged results (see Fig. 7C) for the 18 participants, 14 areas (out of 90) showed this opposite tendency. 12 out of these 14 are actually six pairs of homotopic zones, i.e., pairs of areas that occupy symmetrical zones in each hemisphere. These six pairs of areas are the olfactory, the calcarine (V1), the cuneus (basic visual), the lingual (visual letters), the occipital superior (visual), and the paracentral lobule (motor-sensory), all of them found in both left and right hemispheres. Furthermore, the fusiform in the left hemisphere (facial recognition) and the supplementary motor area in the right hemisphere (control movement). Due to their specific functions, in all cases, it makes sense that these areas were foci of attraction in the wakefulness state.

4. Discussion

In this paper we have proposed a novel mathematical formalism for approximating the time-varying *attractors landscape* (AL) depicted by the dynamical activity of the human brain. In the rich and complex landscape provided by the *Lotka-Volterra* (LV) equations for collaborating species, the energy levels of the *global attractor* can be found by identifying the *globally asymptotically stable solution* (GASS). Our main aim is *not* to provide a better method to discriminate or describe states of awake and sleep, but to validate, for the first time, a theoretical proposal for the study of consciousness states. Although we do not pretend to find a better classification method than those that already exist in the scientific literature, our novel method allows us to clearly characterise and distinguish between different brain states by means of the variability of the associated energy levels, opening up for relevant clinical applications. We defined the Lotka-Volterra transform (LVT) as the time-varying growth rate parameter, $\alpha = \alpha(t)$, that exactly reproduces the empirical BOLD signal. This allowed us to compare the corresponding non-stationary attractor landscapes in wakefulness and sleep conditions.

Lotka-Volterra model was chosen as the simplest model that helped us find an answer to the questions “towards which state is the brain attracted to at a given time point?” and “how do the corresponding attractor landscape surroundings look like?”. Therefore, the choice of the model and the time-dependent parameters (rates of time-dependent growth and fixed structural connectivities) ensure maximum simplicity and coherence. Furthermore, the results show that the method is able to characterise and significantly distinguish (p-values<5%) among the

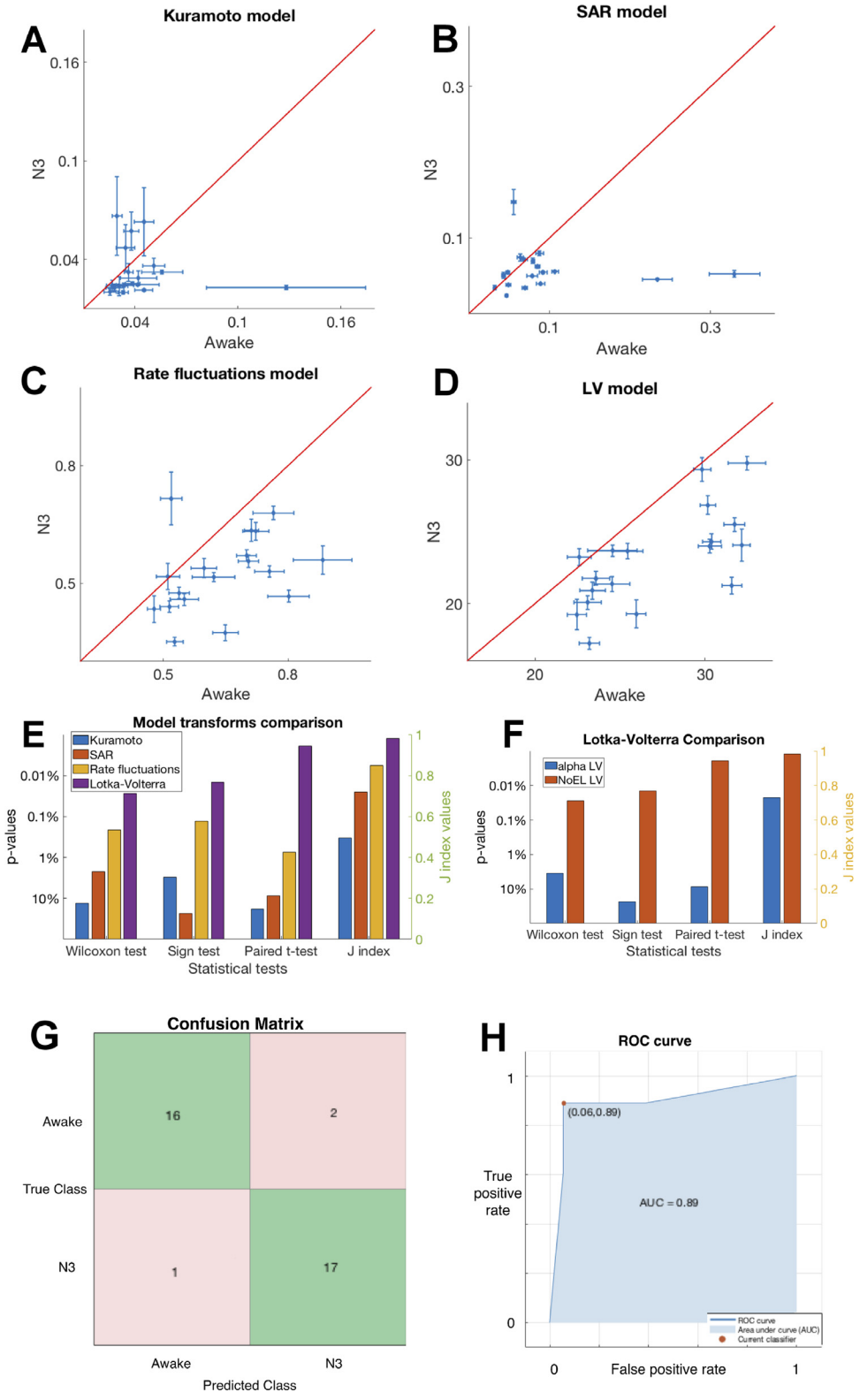

Fig. 6. (**A–E**), Comparisons of NoEL standard deviation among awake (W), and N3 (deep asleep) states using four different model transforms. (**F**), First, we transform BOLD signals into alphas, and then, alphas into energy levels. Here, capacities to distinguish brain states of both transformations are compared. (**G–H**), Classification results training a KNN classifier ($k = 2$) with the mean and the standard deviation of the NoEL obtaining an accuracy of 92%. Data come from 18 subjects in two brain states (W and N3) used as two independent samples.

well-defined brain states of wakefulness (N1, N2 and deep sleep stage N3) in empirical BOLD functional magnetic resonance imaging (fMRI) signals (as measured with concurrent EEG to identify the sleep stages).

Thus, there is a nonlinear transformation from BOLD signals to time-dependent alpha parameters taking into account ninety brain areas. There are many cases, for instance from Ecology or Chemistry, in which a signal produces an alpha vector almost constant in time with our transformation. In that case, all the forward asymptotic behaviour of the system follows a stationary attractor landscape (AL). This is not expected in brain dynamics, and therefore we try to use the time-dependent AL to produce a biomarker (the number of energy levels, NoEL) for the non-stationarity of brain activity.

Still, we have shown that the LVT can be used for the study of brain dynamics, and to compare and distinguish between different brain

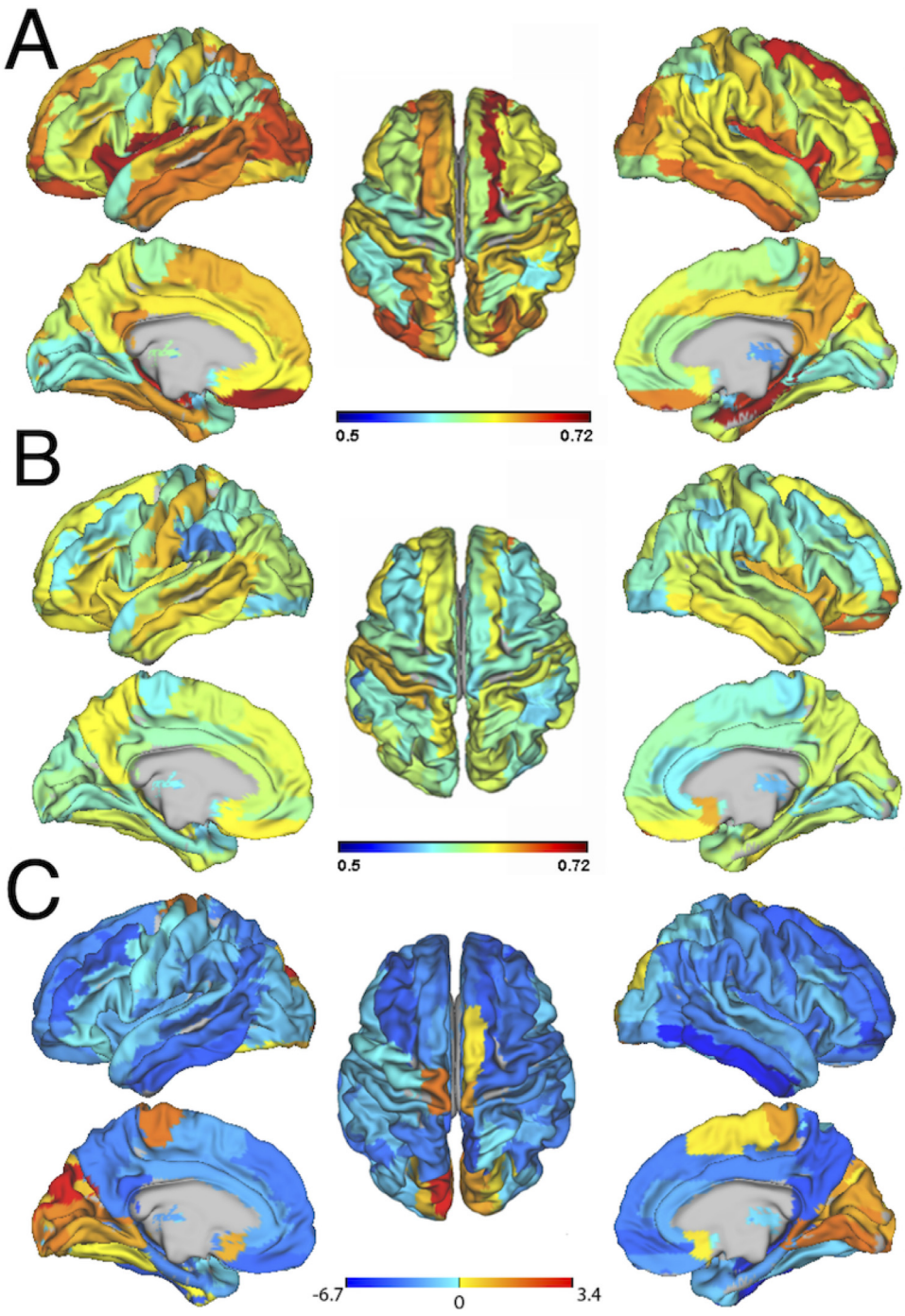

Fig. 7. Frequencies of appearance of each area in the globally asymptotically solution (GASS) in (**A**) deep sleep and in (**B**) awake states averaged over all participants. (**C**), Difference between the averaged frequencies of appearance of each area in the GASS of both states. This difference is expressed in standard error units where the standard error is estimated by the interpersonal variability. Most areas have cold colours, i.e., greater presence in the deep sleep attractor (see Supplementary Materials for individual differences).

states. Indeed, one of the conclusions of this study is that there are significant differences (p-values<5%) in the ALs corresponding to the brain activity of individuals in wakefulness and deep sleep. Before seeing the average probability densities in Fig. 4C, unimodal distributions such as Gaussian distributions could be expected. At least it would be reasonable to expect two similar distributions but with different maxima. However, not only the means of the number of energy levels (NoEL), q, are different, but also the distributions themselves. Besides the very high frequencies obtained for the highest values of q in both distributions, the frequency of the deep sleep NoELs increases with q, while that of wakefulness remains more homogeneous for most values of q.

From its simplicity, the model combines the information from brain activity in each specific area with the coupling with the rest of the brain. Our hypothesis is that the adequate compromise between both sources provides information that is not evident from the experimental data and that allows us to distinguish between brain states. It should be emphasised that the usefulness of our method is not restricted to a narrow range of values of g, neither to a particular filtering range, as shown by the results reported in this study.

4.1. Limitations of the framework

It should be noted that it is important to be careful in interpreting the results of this procedure, since this is still a parametric approach and it could be seriously biased by the choice of parameters (including the model itself). In the first stages of our research it was unclear what

the impact of the choice of time-dependent parameters ($\alpha_i(t)$ or $\gamma_{ij}(t)$) on the LV equations would be. Finally, we used fixed connectivity values γ_{ij} for the conditions (wakefulness, N1, N2 and N3) despite they are known to be associated with distinct levels of effective connectivity. Indeed, in the first stages we used different connectivity matrices for each subject, and even individual effective connectivity. In any case, we believe that the comparison between awake and asleep only makes sense when the same treatment is carried out (which includes the same connectivity matrix) to the different states in each subject. Our intention was to find differences in the attractor with the same mathematical treatment for all participants and states. Furthermore, there is another mathematical reason for this choice: in MT the number of equations n matches the number of parameters to be expressed as functions of time. This requirement is fulfilled by α_i but not by γ_{ij}.

Our formalism does not account for any of the critical structures/circuitry involved in sleep/wake transitions (such as the thalamocortical circuitry) or the external inputs to the brain. Any model that does not account for those factors is bound to overfit. However, recall that we are not modeling but carrying out a transformation of the empirical data to time-dependent parameters. We call this new mathematical tool "transform" because it starts from a $N \times T$ data matrix (N brain areas, T time steps) while the result of the LVT is another $N \times T$ matrix that we call the alphas. Therefore, there is no reduction of information of the dynamics of the system, but rather a transformation to a language that allows us to calculate an attractor at each time instant. In the conceptual framework of modeling, this would be a clear overfitting. In this sense, the MT would be an overfitting by definition because the alphas are defined so that the LV equations with time-dependent parameters exactly comply with the experimental data. But since we are not modeling the dynamics, it should not be considered overfitting in the same way that it does not make sense to consider overfitting the Fourier transform, even though the harmonic oscillator model is involved in the transformation.

We do not aim to characterize the changes in the underlying coupling and to develope a model capable of generating patterns of coupling changes. For us the empirical, real, thalamocortical activity, and of all the other brain areas constitutes an initial data, an input, information that we already have and that we do not intend to model. Our approach is the search for a first approximation to the attractor landscape that explains the experimental data. Furthermore, these attractors are sought at the level of the global brain dynamics when the corresponding brain state is stabilized, and not in the transition between awake and asleep states. In any case, we probably need to perform other more general frameworks. Although this methodology discriminates awake versus sleep states, it is not enough to draw major conclusions on the description of brain dynamics related to these states. Due to the limitations of this framework as a modelization of brain dynamics, this AL should not be taken for other purposes than a biomarker.

4.2. Partial validations

This work can be seen as a contribution to the general idea that attractors are relevant for understanding brain dynamics, but is far from a definitive answer and it is therefore necessary to continue investigating in that direction. Brain dynamics depicts an extremely complex energy landscape and finding a model that predicts its global behavior in the short and long term is a central unsolved problem in neuroscience. Current knowledge and technology do not allow us to confirm whether we are really approaching the state to which the system is attracted to (the attractor) at each time point. It is also true that the mathematical tools used do not need experimental validation because we simply define them that way. In any case, the fact that the average and the standard deviation of the number of levels of these non-stationary attractors can be used to distinguish between awake and deep sleep states can be considered as a first validation.

On the other hand, the results of the classification show that our method not only recognizes the differences between brain states but can also predict these states from a certain BOLD signal with high accuracy. In a paired-samples test, observations are defined as the differences between two sets of values, and each assumption refers to these differences, not the original data values. But while the paired tests were based on differences (how much the mean or the standard deviation of the NoEL increases or decreases in each subject when going from W to N3) in the classification, both samples are considered independent. Therefore, the values of the mean or the standard deviation of the NoEL are directly used and not their differences.

A new partial validation has emerged from the observation that not any MT of any model will lead to significant differences (small p-values) between awake and sleep data. We compared the MT of four different models on the same dataset (SAR, Rate fluctuations, Kuramoto and LV) and found that the LV transform yields the best results. LV has shown a greater ability to distinguish between different states of consciousness compared to the other models when used in the sense of MT. This shows that a given system can be characterized by one MT but not another. It could happen that some systems could not be characterized by any MT. This could be the case of brain activity: no model transform serves to distinguish between the state of consciousness of the subjects. But in this work, we have found at least one MT that not only distinguishes them, but also provides a measure of consciousness.

Our formalism transforms, first, the BOLD signals into alpha values using the LVT, and then, we use these alphas to calculate the structure of the corresponding attractor with its energy levels. Comparison of Fig. 6F shows that the first transformation is not sufficient. Therefore, it is not the case that the data of the brain states are so different that adjusting the model to them results in significant differences in the parameters. This justifies in this formalism the calculation of the attractor structure and its characterization through its energy levels to distinguish well enough between states, since the simple calculation of alphas is not enough to generate a measure of consciousness.

Another partial validation comes from including N1 and N2 in our analyzes. Our results indicate that the same type of differences that exist between Awake and N3 are those found between N1 and N2 and between N2 and N3.

Recently, a novel index of consciousness that works for fMRI data was proposed (Hahn et al., 2021). This index is based on the Fano factor (FF), a measure applied in the analysis of population spiking activity (which captures higher order correlation and global synchrony between discrete events). The GASS also encodes correlations and synchrony among active brain areas and inactive brain areas *but* it does so in the attractor. Furthermore, the mathematical approaches are very different. For example, a) the index in Hahn et al. (2021) uses positive peaks in the BOLD time series, while the growth rates $\dot{u}_i(t)/u_i(t)$ are the main factor in LVT; b) while in LVT the global coupling of each region with the rest of the brain is a very important additional correlation and synchrony factor, the structural connectivity is not considered in Hahn et al. (2021). We computed the Pearson correlation coefficient between the average NoEL and the Beta values of the FF distribution for each subject and brain state, and obtained −0.7562. First, the result is negative because the average NoEL is usually lower in W and N1, whereas the Beta value is higher in those states. Second, it is not a high value, showing that each measure gives a different point of view. Our approach gives better results than those of (Hahn et al., 2021), which managed to classify four subjects with a monotonic increase from awake to N3 sleep, while our method managed to classify five (see Supplementary Materials and Supplementary Fig. 6 in Hahn et al. (2021)). Furthermore, in our case in 88% of the cases (16 out of 18 subjects) the N3 shows more extreme values with respect to the other states, while only 61% (11 out of 18) in Hahn et al. (2021).

In any case, for a definitive validation of this machinery, one needs true models that predict the global behavior of the brain in the short and long term, and to be able to calculate the attractors of these models. As more achievable short-term validations are to be performed, more conscious states in different datasets are needed.

4.3. Explanations of the results

Given that the energy levels can be interpreted not only in terms of energy but also in terms of attraction or stability (see Introduction), this leads to the conclusion that, on average, the approximated non-stationary AL in deep sleep is more stable. Lower stability of the awake state can also be inferred from the greater variability of the NoEL, according to our results. This is in agreement with other studies in which authors claim, using very different methodologies, that the brain exhibits less stability during wakefulness (Jobst et al., 2017).

The mean NoEL $\overline{q}$ is higher when the participants are asleep, as shown in Fig. 4D. It can be explained by using the unstable trivial solution $(0, 0, \ldots, 0)$ as a reference of the energy and considering that when the number of levels increases, the stability of the GASS grows and its energy decreases, the average energy of the deep asleep state is lower than the awake one.

In our results the complexity of the wakefulness state is reflected not in more complex ALs but in the variability of different ALs in this state. Taking the standard deviation as a measure of NoEL distribution variability, Fig. 4E demonstrates that the complexity of an awake individual is higher (except for one case) than in the same individual during deep sleep.

More generally, the conscious state has usually been associated with complexity in different ways. Different measures of the dynamic complexity of a network have been proposed. For instance in Zamora-López et al. (2016), for a given network, its pair-wise correlation matrix reflects the degree of inter-dependencies among the nodes. When the nodes are disconnected or close to independence (equivalent to a small g), no complex collective dynamics emerge and the distribution of cross-correlation values is characterized by a narrow peak in the low-value regime. On the other hand, when the collective dynamics are close to global synchrony (equivalent to a large g), the distribution of cross-correlation values has a peak in the high-value regime. However, it is not a complex state either, since all nodes follow the same behavior. Complexity emerges when the collective dynamics are characterized by intermediate states, between independence and global synchrony, and it is characterized by a broad distribution of correlation values or interdependencies among the node values, so the *functional complexity* is reflected in the variability of the associated distribution. This variability can be defined as normed entropy or as the difference between distribution and uniform distribution quantified as the integral of the absolute value of the difference. Dynamic complexity is thus clearly associated with more uniform distributions. Although our distributions are not made from cross-correlation but from NoEL values, the underlying idea is the same. The pattern of statistical distribution of NoEL in wakefulness (Fig. 4C) can be interpreted as a sign of complexity. We have seen that in deep sleep the probability of a concrete q increases with q. On the contrary, when the participants are awake the frequency remains more uniform when $q \in [1, 89]$.

4.3.1. Alternative explanations

Our results can also be explained based on concepts and results already established in computational neuroscience:

The ALs with the highest NoEL, and therefore possibly those with the highest number of stationary points and trajectories connecting them, are the most repeated for participants both in wakefulness and deep sleep. In addition, in the awake state the maximum NoEL is more frequent than in deep sleep condition (Fig. 4C). Recall that in this case the attractor or GASS has all the components different from zero, that is, the complete brain is active (90 areas) which implies a high degree of effective connectivity. It can be explained considering the decrease in effective connectivity during slow wave sleep (see Jobst et al., 2017).

Generally, the extreme number of energy levels are more frequent in awake compared to deep sleep, as shown in Fig. 4C. These results may be explained as a global effect of a group of local nodes with a high number of links greatly exceeding the average (hubs), driving thus the dynamic system. They can also be interpreted as a higher ability to integrate information whilst the subject is awake and an increased capacity to amplify local perturbations. In contrast, slow-wave deep sleep is associated with a diminished level of integrated information (Tagliazucchi et al., 2013). This result is also explained by the integrated information theory (IIT) of consciousness (Oizumi et al., 2014), which holds that different levels of consciousness must correspond to the brain's ability to integrate information. Many other studies have shown that integration is impaired during non-wakefulness (Deco and Kringelbach, 2014).

Our results also show a decrease of time variability in the deep sleep condition that might be explained as a decrease in the differentiation of brain activity. According to the IIT, this might be thought of as an indicator for diminished conscious awareness (Oizumi et al., 2014).

It is worth mentioning that we have not observed any AL that is exclusive of a particular brain state. Any AL can be found in any of the two states, and it is only through its statistical distribution that we can asses the differences between the brain states. The differences between wakefulness (frequently opened eyes, coordinated body movement and response to the environment) and deep sleep (closed eyes, lack of overt behaviour and absence of response to stimuli) are very well known. However, it has been shown that when wakefulness is prolonged, characteristic OFF periods of the slow wave of sleep can appear locally (Vyazovskiy et al., 2011). In the same way during sleep the frequency of these periods decreases as the sleep goes on. Even local wakefulness characteristics have been shown in global sleep (Nobili et al., 2011). Therefore, it would be expected that at the level of the global brain in which we conducted our study, some of the characteristics of both states are shared while the differences have to be established in a statistical way. Indeed, if we consider the medium-high values of q, characteristic of the sleeping condition, we see that the awake brain can reach these values during some intervals (analogously to a prolonged wakefulness with the characteristic OFF periods that can appear locally Vyazovskiy et al., 2011).

A greater unpredictability of the wakeful brain dynamics can also be considered because there is maximum entropy and minimal information about the state subsequent to the current one. Unpredictability is one of the features of complexity and chaotic dynamics. On the contrary, in deep sleep it is very likely to find the system in a medium-high NoEL attractor landscape, restricting the repertoire of possible dynamics in this state.

Recently it has been shown that BOLD oscillation patterns provide a potential signature of local sleep, where individual fMRI voxels evolves from a mixed-frequency pattern in wakefulness, to a low-frequency (~ 0.05 Hz) oscillation prominent in light sleep, and a high-frequency (~ 0.17 Hz) oscillation prominent in deep sleep (Song et al., 2019). The low-frequency and high-frequency BOLD oscillations could track the occurrences of sleep spindles and slow waves, respectively. This could explain why within this wide range of filters that allow our method to distinguish significantly (p-values<5%) between brain states, the differences are optimal in the range $0.077 - 0.096$ Hz since that range leaves out those characteristic frequencies of BOLD activity during sleep that can interfere with our analysis.

4.4. Are these attractors functionally relevant?

The attractor states are not expected to be directly in the BOLD time series at a given time point, as they correspond to zero flow states. It begs the question of the functional relevance of these attractors and their ultra-slow dynamics (i.e., zero flow), as the faster scale coupling changes ultimately determine the state of the system. If instead of an approximation we had the true AL, this would fully characterize the dynamics of any dynamic system including slow and fast dynamics. The true AL includes all the states of the system, the entire phase space, and all its possible trajectories, not just the ultra-slow dynamics. That is, the knowledge of the AL is equivalent to the complete knowledge of the dynamic system. If we got to know the true AL of a system like

the human brain, we could account not only for the stationary points (zero flow) but also for the faster scale dynamics. However this ideal is unattainable because:

1) The complete knowledge of AL is unmanageable even in simple models such as LV and we reduce it for its mathematical treatment to its structure, that is, to the invariants (usually stationary points with zero-flow) and their connections. In general, a dynamical system evolves away from unstable zero-flow stationary points, but these points are useful to summarize the structure of the AL. We even go one step further and reduce AL to the number of energy levels. Probably the system is moving through different energy levels without necessarily passing near the stationary points that result from our calculations.

2) We are far from being able to calculate the true AL of the human brain. Furthermore, attempts such as the one we present here are conditioned by the temporal and spatial resolution of the measurement devices that produce the empirical data used to calculate AL. The positive counterpart of this is that our framework is flexible in this sense, that is, it is susceptible to being fed by data of different temporal and spatial scales, so the corresponding non-stationary ALs calculated using the LVT would inherit these scales of temporal and spatial resolution. As a consequence of this we can account for the fast scale changes with our $\alpha(t)$ by definition of LVT. Although our tool does not have predictive power, at least we can ensure that our non-stationary AL includes as a solution a trajectory that corresponds to the empirical data and its fast scale dynamics.

Our initial motivation for this research line is that the subject's state of consciousness is related to the AL as a whole, but for operational reasons we reduce the attractor to its structure in a first step and subsequently to its number of levels. Perhaps it would be possible to defend the functional relevance of the ultra-slow dynamics associated with stationary points of the LA to the extent that these stationary points, which are mostly saddle points, repel or attract the state of the system by configuring its fast scale coupling. This can be visualized by imagining that these points curve the phase space, indirectly affecting the dynamics of the system. However, given the limitations of our framework, the functional relevance is limited to the time interval in which the dynamics of the system can be described by a specific AL. After that time interval of the order of a few TR, the AL has changed and it would be new saddle points that would explain the dynamics of the system.

4.5. Relationship with IIT

The global attractor and its structure (the *informational structure,* IS) have previously been associated with the scientific study of consciousness. The IS has been used to determine the level of integrated information for different states (Esteban et al., 2018; Kalita et al., 2019) in the context of the *Integrated Information Theory* (IIT). Nevertheless, here, our proposal is far from the mathematical machinery in IIT, as both the framework and the approach are different. The IIT (Oizumi et al., 2014) proposes a potential route into identifying the essential properties of brain states using five axioms: intrinsic existence, composition, information, integration and exclusion. In other words, given the mechanisms underlying a particular brain state, IIT identifies a brain state with a conceptual structure: an *Informational Object* which is composed of identifiable parts, informative, integrated and maximally irreducible. IIT is thus linked to both *Information Theory* and *Theory of Causality*. IIT is among the leading computational theories of consciousness. It has originally been formulated for binary discrete dynamical systems; thus, IIT consider systems in which the elementary mechanisms are discrete logic gates or linear threshold units and assume that these mechanisms are the ones mediating the strongest causal interactions. The IS of the global attractor has been harnessed to translate IIT's formalism to continuous dynamical systems and constitute a significant departure from the theory's original formulation (Esteban et al., 2018). More specifically the ISs of LV systems have been used to show the dependence between the topology, the value of the parameters and the state with respect to its level of integration (Esteban et al., 2018), as such pointing for the small world configuration of the brain (Bassett and Bullmore, 2006) (although see recent controversies Markov et al., 2013).

4.6. Wakefulness and N1 states

We have also seen that global characteristics of the NoEL distribution such as the mean or standard deviation do not significantly separate awake (W) and N1 states, but that frequencies for certain NoELs serve to distinguish between them suggesting that some subjects could have slightly larger functional complexity in N1 state than W (Fig. 5G). This can be explained by the characteristics shared by N1 and W states. Although a very first and undoubtable sign of the insurgence of sleep is the disappearance of the EEG alpha rhythm within N1, there is an evolution of brain waves that goes from alpha waves in the N1 initial stages to theta waves as the subject enters the N1 phase. This evolution can be explained by the single unified mechanism to generate both, alpha and theta, and other brain rhythms proposed in Galadí et al. (2020). In the comparison between the N1 early phase and the N1 central phase, alpha waves are more powerful in the first and theta waves more important in the second. Thus, in terms of brain wave activity, N1 sleep is associated with both alpha and theta waves. The early portion of N1 sleep produces alpha waves, which are relatively low frequency (8–13Hz), high amplitude patterns of electrical activity (waves) that become synchronized. This pattern of brain wave activity resembles relaxed state, yet awake. It is relatively easy to wake someone from stage 1 sleep; in fact, people aroused from this stage often believe that they have been fully awake. In general, it is difficult to distinguish N1 from W even using EEG, because the distinction is based on suppression of alpha rhythm, and there are subjects who are already poor alpha generators even with eyes closed and awake. In practice, this means that if different evaluators classify EEG between N1 and W, there is a considerable error, and they only agree between 60–70% of the time. N1 bears many similarities to W in that it is characterized by a certain degree of conscious mentality and even visual and auditory content remaining. We think that the communication between the peripheral sensory systems and the cortex is cut due to the deactivation of the thalamus, and that this lack of input makes the conscious content self-generated, that is, more similar to hallucinations than to the conscious content associated with perception of the external world that occurs in waking. But generally speaking, N1 is dynamically similar to W (Tagliazucchi and Laufs, 2014; Tagliazucchi et al., 2013).

The level of wakefulness in N1 state can also be assessed by comparing REM and N1 states. Thus, arousal responses to added inspiratory resistance are similar during REM sleep than during the N1 sleep, while decreases significantly from stage N1 to stage N2 and from N2 to N3 (Gugger et al., 1993). Some authors consider REM dreams experiences similar to wakefulness (Hobson, 2014; Searle et al., 1998) and some results suggest that REMs share characteristics with wakefulness. Thus, REMs during sleep could rearrange discrete epochs of visual-like processing as during wakefulness (Andrillon et al., 2015). Indications from TMS-EEG experiments are that integrated information is high in wakefulness and almost so high in REM sleep (Tononi, 2014). It has even been hypothesized that if the integrated information were higher in REM sleep than in waking, it could be concluded that dreaming was more conscious than wakefulness. Nevertheless, according to IIT it matters not only how much information is integrated but also how it is integrated (Tononi, 2014).

4.7. Comparison with direct transfer entropy

It is interesting to compare our method with other ones based on direct transfer entropy as (Maki-Marttunen et al., 2013). Transfer entropy quantifies the coherence between brain areas from the information theoretic perspective, but in such a way that exchanged information from shared common history and input signals is excluded by appropriate

conditioning of transition probabilities. Thus, transfer entropy is able to distinguish effectively driving and responding elements and to detect asymmetry in the interaction of brain regions. However, in our approach, the information is not quantified in terms of the history of each brain region, but is implicit in the structure of the attractor at each time point. The entropy transfer is calculated from mutual information and mutual conditional information, which, in turn, are based on Shanon's information. This measures the expected value of the surprisal or self-information $log(1/p_X(x))$ and can be interpreted as quantifying the level of "surprise" of a particular outcome. It can be said that it is objective, external information. However, in our work the information is inspired by IIT's ideas as: a) *intrinsic information*, that is, information from the point of view of the system itself, which is described as the "differences that make a difference" within a system and that is expressed in terms of causal power, and b) *integrated information* as information specified by a whole that cannot be reduced to that specified by its parts. Our IS is emergent since it cannot be explained through the dynamics of the separate parts but only through the global dynamics. In IIT causal power is a requirement for the existence of consciousness. Moreover, it is real *in* and *from* itself -from its own intrinsic perspective- without the need for an external observer to come into being. In Esteban et al. (2018) it was proposed that the global attractor and its structure simultaneously express both aspects of IIT: the *causal power* of the system by configuring the trajectories of the system in the phase space and *integration* by being a characterization of the system as a whole.

4.8. Translational impact

The scope of this work should not be reduced to the theoretical plane among other reasons because:

1. The experimental data are the starting point.
2. The theoretical framework can be put into practice without simplifying the theory.
3. We can classify the subjects by training a classifier, obtaining high percentages of accuracy. This means that by simply measuring the BOLD signal of a subject and calculating through our formalism the frequency with which it reaches, for example, 3 and 59 energy levels respectively for a few minutes, we can predict its state of consciousness with 92% accuracy.
4. We have developed a measure of consciousness that distinguishes W, N1, N2 and N3 with p-values below 1.39% (see Fig. 5).
5. The local attractors that we obtain are not abstract entities but real brain states in which some brain regions are active while others are not.
6. It must also considered that many of the measures of consciousness in the scientific literature are defined for theoretical systems but difficult to apply in practice. For example, phi in IIT 3.0 is applicable only to discrete Markovian systems (see Oizumi et al., 2014). Other measures can be estimated for real data using empirical distributions only if stationarity can be assumed. Non-stationarity is a remaining important challenge, in many practical scenarios. For long data segments, it can be unrealistic to assume that all the statistics are constant throughout. For shorter data segments, one cannot be confident that the system has explored all the states (see Mediano et al., 2019). However, our measure is designed to be applied directly to non-stationary empirical data.

4.9. Future directions

Here we characterize the structure of the AL through the NoEL, although this leaves a high amount of (possibly) crucial information about the entire structure left to be explored in future works. The global dynamics underlying brain states emerge from complex interactions among brain regions. By describing the topological structure of the global attractor at each moment in time, we could be able to classify different brain states by using the statistics across time of these exact structures until now hidden. Given the potential of this framework, we would be able to classify the neuroimaging data from different classes of comatose patients. This approach has the potential to provide new insights into the causal mechanistic principles lying beneath the complex dynamics defining brain states.

The concept of non-stationary AL with stationary points moving in the phase space and changing their stability could be harnessed to describe multistability or metastability and could be even a useful tool to analyze the functional connectivity dynamics. For example, metastability is usually measured with the standard deviation σ_R of the Kuramoto order parameter R, where R is the module of the complex number $\frac{1}{n}\sum_{j=1}^{n} e^{i\theta_j}$ (Shanahan, 2010). However, what σ_R really describes is a variability in the overall synchronization of the system. An alternative is to use the standard deviation of the NoEL, which assesses the tendency of the system to change local attractors and could be called *structural metastability*.

The new concept of MT allows simple models to be applied to complex empirical systems. It does not only unify trivial cases such as the instantaneous velocity, the curvature of a plane curve or the torsion of a non-planar curve under the same conceptual framework, but also projects in all fields of knowledge in which any system, simple or complex, theoretical or empirical, defined on a network or not, can be characterized by time-dependent values of the parameters. Each different model opens different possibilities in countless practical and theoretical applications. Indeed, a Kuramoto Transform in which the natural frequencies were the parameters to be fitted in each time interval would provide a non-stationary landscape in which the GASSs would be periodic orbits, as opposed to the stationary points of the LVT.

4.10. Conclusions

The main contribution of this work is a mathematical and theoretical framework for approximating the non-stationary attractor landscape of a brain state. This framework is able to find significant differences between brain states using empirical neuroimaging data. In the future, further steps in this regard include finding out what lies below this explanation of the complex dynamical landscape. The theoretical framework proposed is potentially relevant for the development of the study of consciousness, and of biomarkers in translational applications, especially in the context of patients with neuropsychiatric disorders and with different levels of coma.

Declaration of Competing Interest

The datasets analyzed during the current study are not publicly available due to constraints imposed by the ethics approval but are available from the corresponding author on reasonable request.

Credit authorship contribution statement

J.A. Galadí: Conceptualization, Methodology, Software, Formal analysis, Writing – original draft, Visualization, Writing – review & editing. **S. Silva Pereira:** Conceptualization, Visualization, Writing – review & editing. **Y. Sanz Perl:** Writing – review & editing. **M.L. Kringelbach:** Investigation, Visualization, Writing – review & editing. **I. Gayte:** Conceptualization, Writing – review & editing. **H. Laufs:** Investigation, Writing – review & editing. **E. Tagliazucchi:** Investigation, Writing – review & editing. **J.A. Langa:** Conceptualization, Supervision, Writing – review & editing. **G. Deco:** Conceptualization, Supervision, Writing – review & editing.

Acknowledgments

J.A.G., I.G. and J.A.L have been partially supported by Spanish Ministerio de Economía y Competitividad and FEDER, projects MTM2015-

63723-P, PGC2018-096540-B-I00, Proyecto US-1254251 del Fondo Europeo de Desarrollo Regional (FEDER) y la Consejería de Economía, Conocimiento, Empresas y Universidad de la Junta de Andalucía, dentro del Programa Operativo FEDER 2014-2020 and Proyecto PAIDI 2020 P20_00592. S.S.P. is supported by the Research Project PGC2018-096641-B-I00 (Ministerio de Ciencia, Innovación y Universidades / Agencia Estatal de Investigación /FEDER, UE). G.D. is supported by the Spanish Research Project PSI2016-75688-P (Agencia Estatal de Investigacíon/Fondo Europeo de Desarrollo Regional, European Union); by the European Union's Horizon 2020 Research and Innovation Programme under Grant Agreements 720270 (Human Brain Project [HBP] SGA1) and 785907 (HBP SGA2); and by the Catalan Agency for Management of University and Research Grants Programme 2017 SGR 1545. M.L.K. is supported by the European Research Council Consolidator Grant: CAREGIVING (615539) and Center for Music in the Brain, funded by the Danish National Research Foundation (DNRF117). H.L. and data acquisition were supported by the Bundesministerium für Bildung und Forschung (grant no. 01 EV 0703); H.L. and E.T. by the LOEWE Neuronale Koordination Forschungsschwerpunkt Frankfurt (NeFF); H.L. also by Christian-Albrechts-University Kiel and the CRC1261 (Deutsche Fors-chungsge-meinschaft). We thank Astrid Morzelewski for sleep scoring of the EEGs.

Supplementary material

Supplementary material associated with this article can be found, in the online version, at 10.1016/j.neuroimage.2021.118551.

References

Afraimovich, V., Zhigulin, V., Rabinovich, M., 2004. On the origin of reproducible sequential activity in neural circuits. Chaos 14 (4), 1123–1129. doi:10.1063/1.1819625.

Andrillon, T., Nir, Y., Cirelli, C., Tononi, G., Fried, I., 2015. Single-neuron activity and eye movements during human rem sleep and awake vision. Nat. Commun. 6 (1), 7884. doi:10.1038/ncomms8884.

Aragao-Costa, E., Caraballo, T., Carvalho, A., Langa, J., 2012. Continuity of Lyapunov functions and of energy level for a generalized gradient semigroup. Topol. Methods Nonlinear Anal. 39 (1), 57–82.

Bassett, D., Bullmore, E., 2006. Small-world brain networks. Neuroscientist 12 (6), 512–523. doi:10.1177/1073858406293182. PMID: 17079517

Bortolan, M., Carvalho, A., Langa, J., 2020. Attractors under autonomous and non-autonomous perturbations. Mathematical Surveys and Monographs. American Mathematical Society.

Cardanobile, S., Rotter, S., 2011. Emergent properties of interacting populations of spiking neurons. Front. Comput. Neurosci. 5, 59. doi:10.3389/fncom.2011.00059.

Carvalho, A., Langa, J., Robinson, J., 2012. Attractors for infinite-dimensional non-autonomous dynamical systems. Applied Mathematical Sciences. Springer New York.

Cottle, R., Pang, J., Stone, R., 1992. The linear complementarity problem. Classics in Applied Mathematics. Society for Industrial and Applied Mathematics (SIAM, 3600 Market Street, Floor 6, Philadelphia, PA 19104).

Deco, G., Cabral, J., Woolrich, M., Stevner, A., van Hartevelt, T., Kringelbach, M., 2017. Single or multiple frequency generators in on-going brain activity: a mechanistic whole-brain model of empirical meg data. NeuroImage 152, 538–550. doi:10.1016/j.neuroimage.2017.03.023.

Deco, G., Cruzat, J., Cabral, J., Tagliazucchi, E., Laufs, H., Logothetis, N., Kringelbach, M., 2019. Awakening: predicting external stimulation forcing transitions between different brain states. PNAS 116 (36), 18088–18097.

Deco, G., Jirsa, V., 2012. Ongoing cortical activity at rest: criticality, multistability, and ghost attractors. J. Neurosci. 32 (10), 3366–3375. doi:10.1523/JNEUROSCI.2523-11.2012. http://www.jneurosci.org/content/32/10/3366.full.pdf

Deco, G., Kringelbach, M., 2014. Great expectations: using whole-brain computational connectomics for understanding neuropsychiatric disorders. Neuron 84 (5), 892–905. doi:10.1016/j.neuron.2014.08.034.

Esteban, F., Galadí, J., Langa, J., Portillo, J., Soler-Toscano, F., 2018. Informational structures: a dynamical system approach for integrated information. PLoS Comput. Biol. 14 (9), 1–33. doi:10.1371/journal.pcbi.1006154.

Fukai, T., Tanaka, S., 1997. A simple neural network exhibiting selective activation of neuronal ensembles: from winner-take-all to winners-share-all. Neural Comput. 9 (1), 77–97. doi:10.1162/neco.1997.9.1.77.

Galadí, J., 2020. Dynamical systems applied to consciousness and brain rhythms in a neural network. Department of Differential Equations and Numerical Analysis. University of Seville Ph.D. thesis.

Galadí, J., Torres, J., Marro, J., 2020. Emergence and interpretation of oscillatory behaviour similar to brain waves and rhythms. Commun. Nonlinear Sci. Numer. Simul. 83, 105093. doi:10.1016/j.cnsns.2019.105093.

Galán, R.F., 2008. On how network architecture determines the dominant patterns of spontaneous neural activity. PLoS ONE 3 (5), 1–10. doi:10.1371/journal.pone.0002148.

Golos, M., Jirsa, V., Dauce, E., 2016. Multistability in large scale models of brain activity. PLoS Comput. Biol. 11 (12), 1–32. doi:10.1371/journal.pcbi.1004644.

Gugger, M., Bögershausen, S., Schäffler, L., 1993. Arousal responses to added inspiratory resistance during rem and non-rem sleep in normal subjects.. Thorax 48 (2), 125–129. doi:10.1136/thx.48.2.125. https://thorax.bmj.com/content/48/2/125.full.pdf

Hahn, G., Zamora-López, G., Uhrig, L., Tagliazucchi, E., Laufs, H., Mantini, D., Kringelbach, M.L., Jarraya, B., Deco, G., 2021. Signature of consciousness in brain-wide synchronization patterns of monkey and human fMRI signals. NeuroImage 226, 117470. doi:10.1016/j.neuroimage.2020.117470.

Hale, J., 1988. Asymptotic behavior of dissipative systems. Mathematical Surveys and Monographs. American Mathematical Society.

Hobson, J.A., 2014. Introduction. Springer International Publishing, Cham, pp. 3–7.

Jobst, B., Hindriks, R., Laufs, H., Tagliazucchi, E., Hahn, G., Ponce-Alvarez, A., Stevner, A., Kringelbach, M., Deco, G., 2017. Increased stability and breakdown of brain effective connectivity during slow-wave sleep: mechanistic insights from whole-brain computational modelling. Sci. Rep. 7 (1), 4634. doi:10.1038/s41598-017-04522-x.

Kalita, P., Langa, J., Soler-Toscano, F., 2019. Informational structures and informational fields as a prototype for the description of postulates of the integrated information theory. Entropy 21 (5). doi:10.3390/e21050493.

Kuramoto, Y., 1975. Self-entrainment of a population of coupled non-linear oscillators. In: Araki, H. (Ed.), International Symposium on Mathematical Problems in Theoretical Physics. Springer Berlin Heidelberg, Berlin, Heidelberg, pp. 420–422.

Maki-Marttunen, V., Diez, I., Cortes, J., Chialvo, D., Villarreal, M., 2013. Disruption of transfer entropy and inter-hemispheric brain functional connectivity in patients with disorder of consciousness. Front. Neuroinform. 7, 24. doi:10.3389/fninf.2013.00024.

Markov, N., Ercsey-Ravasz, M., Essen, D.V., Knoblauch, K., Toroczkai, Z., Kennedy, H., 2013. Cortical high-density counterstream architectures. Science 342 (6158), 1238406. doi:10.1126/science.1238406.

Marple, L., 1999. Computing the discrete-time "analytic" signal via fft. IEEE Trans. Signal Process. 47 (9), 2600–2603. doi:10.1109/78.782222.

Mediano, P.A., Seth, A.K., Barrett, A.B., 2019. Measuring integrated information: comparison of candidate measures in theory and simulation. Entropy 21 (1). doi:10.3390/e21010017.

Messe, A., Rudrauf, D., Giron, A., Marrelec, G., 2015. Predicting functional connectivity from structural connectivity via computational models using MRI: an extensive comparison study. NeuroImage 111, 65–75. doi:10.1016/j.neuroimage.2015.02.001.

Murray, J., 2013. Mathematical biology. Biomathematics. Springer Berlin Heidelberg.

Nir, Y., Massimini, M., Boly, M., Tononi, G., 2013. Sleep and Consciousness. Springer Berlin Heidelberg, Berlin, Heidelberg, pp. 133–182.

Nobili, L., Ferrara, M., Moroni, F., Gennaro, L.D., Russo, G.L., Campus, C., Cardinale, F., Carli, F.D., 2011. Dissociated wake-like and sleep-like electro-cortical activity during sleep. NeuroImage 58 (2), 612–619. doi:10.1016/j.neuroimage.2011.06.032.

Oizumi, M., Albantakis, L., Tononi, G., 2014. From the phenomenology to the mechanisms of consciousness: integrated information theory 3.0. PLoS Comput. Biol. 10 (5), 1–25. doi:10.1371/journal.pcbi.1003588.

Rao, C., 2009. Linear statistical inference and its applications, 2nd ed. (With Cd). Wiley Series in Probability and Statistics. Wiley India Pvt. Limited.

Robinson, J., Crighton, D., Ablowitz, M., 2001. Infinite-dimensional dynamical systems: an introduction to dissipative parabolic PDEs and the theory of global attractors. Cambridge Texts in Applied Mathematics. Cambridge University Press.

Searle, J., Dennett, D., Chalmers, D., 1998. The Mystery of Consciousness. Granta Books.

Shanahan, M., 2010. Metastable chimera states in community-structured oscillator networks. Chaos 20 (1), 013108. doi:10.1063/1.3305451.

Song, C., Boly, M., Tagliazucchi, E., Laufs, H., Tononi, G., 2019. Bold signatures of sleep. bioRxiv doi:10.1101/531186. https://www.biorxiv.org/content/early/2019/01/26/531186.full.pdf

Tagliazucchi, E., Laufs, H., 2014. Decoding wakefulness levels from typical fMRI resting-state data reveals reliable drifts between wakefulness and sleep. Neuron 82 (3), 695–708. doi:10.1016/j.neuron.2014.03.020.

Tagliazucchi, E., von Wegner, F., Morzelewski, A., Brodbeck, V., Jahnke, K., Laufs, H., 2013. Breakdown of long-range temporal dependence in default mode and attention networks during deep sleep. Proc. Natl. Acad. Sci. 110 (38), 15419–15424. doi:10.1073/pnas.1312848110. https://www.pnas.org/content/110/38/15419.full.pdf

Takeuchi, Y., 1996. Global Dynamical Properties of Lotka-Volterra Systems. World Scientific.

Takeuchi, Y., Adachi, N., 1980. The existence of globally stable equilibria of ecosystems of the generalized volterra type. J. Math. Biol. 10 (4), 401–415. doi:10.1007/BF00276098.

Tononi, G., 2014. How Does Your PHI Formula Deal with the Evidence that Consciousness Is State Dependent? More Specifically, if PHI Were Higher in REM Sleep Than in Waking, Would You Conclude That Dreaming Was More Conscious Even Than Waking?. Springer International Publishing, Cham, pp. 215–217.

Tononi, G., Sporns, O., Edelman, G.M., 1994. A measure for brain complexity: relating functional segregation and integration in the nervous system. Proc. Natl. Acad. Sci. 91 (11), 5033–5037. doi:10.1073/pnas.91.11.5033. https://www.pnas.org/content/91/11/5033.full.pdf

Tzourio-Mazoyer, N., Landeau, B., Papathanassiou, D., Crivello, F., Etard, O., Delcroix, N., Mazoyer, B., Joliot, M., 2002. Automated anatomical labeling of activations in SPM using a macroscopic anatomical parcellation of the MNI MRI single-subject brain. NeuroImage 15 (1), 273–289. doi:10.1006/nimg.2001.0978.

Vohryzek, J., Deco, G., Cessac, B., Kringelbach, M.L., Cabral, J., 2020. Ghost attractors in spontaneous brain activity: recurrent excursions into functionally-relevant bold phase-locking states. Front. Syst. Neurosci. 14, 20. doi:10.3389/fnsys.2020.00020.

Vyazovskiy, V., Olcese, U., Hanlon, E., Nir, Y., Cirelli, C., Tononi, G., 2011. Local sleep in awake rats. Nature 472, 443–447.

Yeung, M., Strogatz, S., 1999. Time delay in the Kuramoto model of coupled oscillators. Phys. Rev. Lett. 82 (3), 648–651. doi:10.1103/PhysRevLett.82.648. Cited By 405

Yuan, R.-S., Ma, Y.-A., Yuan, B., Ao, P., 2014. Lyapunov function as potential function: a dynamical equivalence. Chin. Phys. B 23 (1), 010505. doi:10.1088/1674-1056/23/1/010505.

Zamora-López, G., Chen, Y., Deco, G., Kringelbach, M., Zhou, C., 2016. Functional complexity emerging from anatomical constraints in the brain: the significance of network modularity and rich-clubs. Sci. Rep. 6, 38424.

Zhou, J.X., Aliyu, M.D.S., Aurell, E., Huang, S., 2012. Quasi-potential landscape in complex multi-stable systems. J. R. Soc. Interface 9 (77), 3539–3553. doi:10.1098/rsif.2012.0434. https://royalsocietypublishing.org/doi/pdf/10.1098/rsif.2012.0434

Further readings

Lagzi, F., Atay, F.M., Rotter, S., 2019. Bifurcation analysis of the dynamics of interacting subnetworks of a spiking network. Sci. Rep. 9, 11397. doi:10.1038/s41598-019-47190-9.

Lagzi, F., Rotter, S., 2015. Dynamics of Competition between Subnetworks of Spiking Neuronal Networks in the Balanced State. PLoS ONE 10(9): e0138947. doi:10.1371/journal.pone.0138947.